UNIVERSITY OF GHANA

COLLEGE OF BASIC AND APPLIED SCIENCES

EFFECTS OF IMMOBILIZATION DEVICES ON SKIN DOSES AND DOSES IN THE BUILD-UP REGIONS FOR HIGH ENERGY PHOTON BEAMS

BY

BISMARK DJAN

(10598536)

THIS THESIS/DISSERTATION IS SUBMITTED TO THE UNIVERSITY OF GHANA, LEGON IN PARTIAL FULFILMENT OF THE REQUIREMENT FOR THE AWARD OF MPHIL MEDICAL PHYSICS DEGREE

JULY, 2018

DECLARATION

This thesis is the result of a research work undertaken by Bismark Djan in the Department of Medical Physics, School of Nuclear and Allied Sciences, University of Ghana – Legon. The research was done under the able supervision of Prof. J. H. Amuasi, Dr. Francis Hasford, and Mr. George Felix Acquah all from the Department of Medical Physics.

It is my conviction that, no part of this research work has been presented in part or whole to any other institution or university for the award of a diploma, or degree at any level. Accordingly, other works and/or researches done by other researchers cited in this work have been duly acknowledged under references.

…….. Date ……
Bismark Djan
(Student's ID: 10598536)

…….. Date ……
Dr. Francis Hasford
(Principal Supervisor)

…….. Date ……
Prof. J. H. Amuasi
(Co-Supervisor)

…….. Date ……
Mr. George Felix Acquah
(Co-Supervisor)

ABSTRACT

This study presents the significant increase in skin dose caused by the presence of thermoplastic immobilizing masks used for positioning and immobilization of patients during cancer treatments in the head and neck region. Made from organic materials, thermoplastics become soft and pliable when heated and forms a rigid replication of the patient's anatomy as it cools down. The use of the mask plays a key role in achieving the therapeutic aim in head and neck treatments but can as well lead to a rise in surface dose. The purpose of this research is to examine and analyze the effects of thermoplastic masks used as immobilization devices on skin and the build-up region doses for a 6 MV Three Dimensional Conformal Radiotherapy plan. Measurements in the solid water phantom coupled with an electrometer and a Roos type ionization chamber at the surface (skin), the d_{max} (1.6 cm) and a specified depth of 10 cm of the 6 MV photon beam were made and recorded employing the isocentric technique for known varying field sizes with 100 MU. Measurements with or without the mask were also made on the phantom. GafChromic films were also used to assess the skin dose and d_{max} and compared to the measured values. Surface dose increased significantly due to the presence of the thermoplastic masks. It was observed that the estimated surface doses with the presence of the thermoplastic mask were consistently larger than those without the mask. Due to the presence of the thermoplastic mask during measurements, the dose in the build-up region increased, subsequently shifting the depth of maximum dose, d_{max}, to shallower depths to the skin surface. For a field size of 10 x 10 cm^2, an increase in skin dose of **0.21, 0.13 and 0.05 Gy** was estimated for the unstretched mask, the 5 cm stretched mask and the 10 cm stretched mask respectively, which was ascribed to the "bolus" effect of

the thermoplastic masks. For the various field sizes, the skin dose increased by an average factor less than **1%** for the different mask stretches. However, a variation within 1% was recorded although the skin dose decreased as the mask was extended. The thermoplastic factor at the skin surface was also found to increase with an increasing mask thickness and for a particular mask type (unstretched, 5 cm stretched, or 10 cm stretched) the thermoplastic factor decreased with increasing field size. The discrepancies obtained using the GafChromic films varied significantly with those obtained using the ionization chamber which was associated with the heterogeneous composition of the film arising from the manufacturing process. The skin-sparing effect which is an advantage for megavoltage beams was not achieved due to the presence of the masks.

DEDICATION

This thesis work is dedicated to God Almighty for love, care, provisions, encouragements, strength, protection, and blessings He has given me throughout my education and above all, for the wisdom, He has been granting me since secondary school till now. Also, I dedicate this work to my irreplaceable family for their love, care, encouragements, support and prayers throughout my education and most especially to my sister Mrs. Esther Anokye.

ACKNOWLEDGMENTS

My first and foremost thanks and appreciation go to God Almighty for protecting and guiding me, giving me the sound health, wisdom, knowledge and providing me with all that I needed throughout this research work. May His sovereign name be praised now and forever more.

I am very much grateful to the International Atomic Energy Agency for making it possible for me to undertake this Master of Philosophy Degree programme in Medical Physics here in Ghana.

I sincerely salute my able supervisors, Prof. J.H. Amuasi, Dr. Francis Hasford, and Mr. George Felix Acquah for their continued pieces of advice, corrections, directions, comfort, sacrifices and above all the love and commitments they had in helping me through with my work. No word can express my joy at having you as my team of supervisors, I truly appreciate your support.

Also, to my parents and siblings, I am very much grateful for all the support, advice, encouragements and love you gave me during my entire life in school. I pray for Gods blessings for you all.

Lastly, my special thanks go to my Head of Department, Dr. Francis Hasford who is also my principal supervisor and all the Lecturers for their continued encouragements and motivations.

TABLE OF CONTENTS

LIST OF FIGURES

LIST OF TABLES

LIST OF ABBREVIATIONS

SGMC	Sweden Ghana Medical Centre
MPHIL	Master of Philosophy
ICRU	International Commission on Radiation Units and Measurements
MU	Monitor Units
3DCRT	Three-Dimensional Conformal Radiotherapy
TG	Task Group
TPS	Treatment Planning System
SAD	Source to Axis Distance
CT	Computed Tomography
SSD	Source to Surface Distances
PDD	Percentage Depth Dose
IMRT	Intensity-Modulated Radiation Therapy
ICRP	International Commission on Radiological Protection
MV	Mega Voltage
AAPM	American Association of Physicist in Medicine
CPE	Charge Particle Equilibrium
D_{max}	Depth of Maximum Dose
LINACs	Linear Accelerators
TCP	Tumor Control Probability
IEC	International Electrotechnical Commission
NTCP	Normal Tissue Complication Probability

TIFF	Tagged Image File Format
TLD	Thermoluminescent dosimeter
RGB	Red, Green and Blue
EF-IMRT	Extended Field Intensity-Modulated Radiotherapy
TMR	Tissue Maximum Ratio
OD	Optical Density
PMMA	Polymethylmethacrylate
UV	Ultra Violet
PTV	Planning Target Volume
IAEA	International Atomic Energy Agency
CRT	Conformal Radiation Therapy
Co-60	Cobalt-60 Teletherapy unit
QC	Quality Control
TF	Thermoplastic Factor
EBTXD	EBT-eXtended Dose

CHAPTER ONE

INTRODUCTION

1.1 Background

Ever since Wilhelm Conrad Roentgen begun with the discovery of X-rays on the 8th November 1895 at the University of Wurzburg and Antoine Henri Becquerel coined the radioactivity phenomenon in 1896, cancer treatments have been appreciated through the use of ionizing radiation. (Podgorsak & Rosenberg, 2008) stated that "radiotherapy, also known as radiation therapy, radiation oncology or therapeutic radiology, is one of the three major modalities used in the treatment of cancers, where electromagnetic and particle radiations are used, with the other two being surgery and chemotherapy". Radiation therapy subsequently has gained recognition and has tremendously improved and developed into one of the important specialized medical fields. (Podgorsak & Rosenberg, 2008) have also stated that "X-rays are mostly used in diagnostic radiology for diagnosing diseases and in radiation oncology for the treatment of cancerous tumors".

Radiation therapy is generally characterized by two major forms considering the distance between the radiation source and the tumor, to be treated. Brachytherapy "is a method of treatment in which sealed radioactive sources are used to deliver radiation at a short distance by interstitial, intracavitary, or surface application" as stated by (Khan, 2014). In this method of therapy, the high radiation dose is delivered locally to the tumor with rapid dose fall-off in the surrounding normal tissue. The second form of radiation therapy is known as external beam radiotherapy. (Podgorsak & Rosenberg, 2008) describes this as a type of radiation therapy which has the radiation source at a distance away from the patient and the tumor target within the patient is irradiated with an external radiation

beam. Most of the external beam radiation therapy is performed with photon beams, some with electron beams and a very small fraction with more exotic particles such as heavy ions, protons or neutrons.

Studies by (Sweeney et al., 1998) have shown that the accurate delivery of a prescribed radiation dose to a target tumor while sparing surrounding critical and normal tissues, is the key objective of radiotherapy. The International Commission on Radiation Units and Measurements (ICRU) recommends that to obtain this accuracy, it is required that the error in total dose be within ±5% (Musolino, 2000). Figure 1 illustrates the concept of therapeutic ratio explained by (Williams & Thwaites, 2000) as delivering the highest probable dose to the tumor and thus the maximum probability of complete tumor regression.

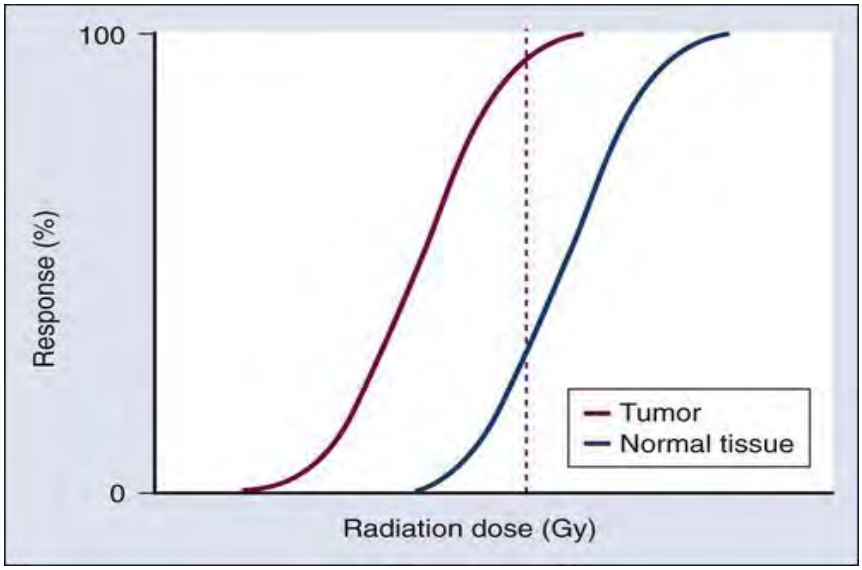

Figure 1. 1: An illustration of the concept of therapeutic ratio. Image from ("Basics of Radiation Therapy | Clinical Gate," 2015)

Radiotherapeutic success is most probable when the two curves in Figure 1 are widely separated (Williams & Thwaites, 2000). The further the normal tissue complication

probability (NTCP) curve is to the right of the tumor control probability curve (TCP), the greater the therapeutic ratio and the lesser the treatment complications.

The prescribed treatment can either be for curative or palliative intent. In the case of curative purpose, the side effects are sometimes unavoidable, but they are accepted as an inevitable part of the cure. On the other hand, (Tabakov et al., 2008) stated that "where cure from radical treatment is unlikely, palliative treatment can alleviate painful or distressing symptoms and restore a higher degree of life quality for patients". A target dose uniformity within +7% and -5% is recommended by the ICRU Report number 50 for the radiation dose delivered to a precise prescription point within the target (Jones, 1994).

In external beam radiation therapy, medical linear accelerators and Cobalt-60 units are used for cancer treatments and the procedures of treatment commonly rely on different conditions such as the;

- Shape, size, and position of the cancerous cells.
- Location of sensitive or critical organs within the locality of the target volume (that is, sparing of normal tissues) and
- Financial constraints and the quest for optimization of radiation dose to the target volume.

(Khan, 2014) indicates that "skin-sparing effect is one of the most desired features of megavoltage beams, and all effort should be focused toward preserving this effect when irradiating normal skin". However, this effect may be reduced or even lost if the radiation beam is extremely contaminated with secondary electrons. Consequently, skin dose should be negligible during this treatment delivery, but this is never achieved because it

depends on secondary electrons (Yadav et al. 2009). These secondary electrons are mostly produced by the interaction of photons with some scattering materials such as collimator jaws, air, patient's skin and beam modifiers. (Nilsson & Brahme, 1986) has shown in their studies that the air column under block tray has a more substantial contribution at lower energies.

(Prabhu, 2012) has shown that positioning and immobilization of patients are the most crucial parts of radiotherapy treatment. Therefore, in order to achieve this therapeutic aim in the head and neck areas of cancer treatment, patients undertaking radiation therapy must be well immobilized. Without proper immobilization such as the use of thermoplastic masks, a patient is probably at risk for wrong or improper treatment and this can result in unwanted side effects. In his study, (Meyer, 2014) stated that “a skin condition called radiation dermatitis is one of the most common side effects of radiation treatment and can range from a mild, red rash (erythema) and itchy, peeling or flaking skin to a more severe reaction with blisters and wet, peeling skin”.

Thermoplastic is a plastic material (polymer) which turn out to be pliable or mouldable above a certain temperature and hardens upon cooling. The main goal of a thermoplastic mask is to provide a dependable method for accurate patient positioning and immobilization during radiation head and neck treatments as well as patient repositioning from one treatment to another and improving patient comfort. The thermoplastic mask is first placed in warm water at a specified temperature to soften it and make it pliable, then pulled over the patient’s face and moulded to the contours of his/her anatomy. As the thermoplastic mask cools down, a firm replication of the patient’s anatomy is then produced, and the thermoplastic mask is then fastened directly to the treatment couch.

Head and neck cancer treatments require a high degree of accuracy and the use of these thermoplastic masks provides the required accuracy. It is, therefore, important to determine its effect on patient's skin and build-up region doses. Figure 2 shows the effect of thermoplastic masks on a patient's skin after five weeks of head and neck cancer treatment.

Figure 1. 2: Physical evidence of the effects of a thermoplastic mask on patient skin showing broken skin after five weeks of radiation treatment. Image obtained from (Thomas, n.d.)

(Hsu et al., 2008), in their study, indicated that accurate evaluations of surface and superficial doses in radiation therapy can present keen information for clinical deliberation and at the same time controlling severe skin toxicity, particularly for breast and head-and-neck treatments since dose at the skin is primarily as a result of electron contamination arising from the flattening filter, beam modifiers, and air.

This study is aimed at assessing the dosimetric effects caused by thermoplastic immobilizing devices on skin and build-up region doses for a 6 MV photon beam using a Roos Chamber type 34001 coupled with UNIDOS Electrometer and an EBT3 GafChromic film for different field sizes for patients undergoing cancer treatments in the

head and neck using a medical linear accelerator at the Sweden Ghana Medical Center in Accra.

1.2 Problem Statement

In radiation therapy, there is the possibility of encountering several problems since tumors in areas like head and neck are in close proximity to healthy tissues/critical organs and the radiation has to travel through these healthy tissues before reaching the target volume. Consequently, patients are required to be properly immobilized using immobilization devices to provide precision/accuracy during treatments, enhance reproducibility from one treatment fraction to another, to reduce daily setup errors and also increase patient comfort.

In view of the proximity of the tumor to the surrounding critical organs and normal tissues with comparatively limited intra-fractional motion in head and neck cancers, proper immobilization technique will allow smaller treatment margins and reduce the side effects.

However, recent works have shown that the use of these immobilization devices (thermoplastic mask) tends to attenuate part of the radiation beam and as a result, increasing skin toxicity and the dose to the build-up region. From literature, the presence of the thermoplastic mask tends to have some effects on the dosimetric outcomes (skin or surface dose, dose at maximum depth, and at a depth of d = 10 cm). Because of the uneven stretching of the heated thermoplastic mask, one ends up having a mask with varying holes which also contributes to dosimetric effects on the patient. This can,

however, have an effect on the quality of life of the patients after treatment. Since these effects are mostly ignored in practice, it is, therefore, important to analyze their impacts on radiation therapy for head and neck cancer treatments.

This study thus seeks to investigate the operational challenges of using thermoplastic immobilization mask and find out how its dosimetric effects can be reduced.

1.3 Objectives

The main aim of this study is to examine and analyze the effects of thermoplastic masks used as immobilizing devices on the skin and the build-up region doses. The study involves 3D conformal radiotherapy (CRT) plan for patients receiving head and neck cancer treatments using 6 MV external radiation therapy (medical linear accelerator) with a flat ionization chamber and EBT3 GafChromic films dosimetry.

The specific objectives are to:

1. Determine the LINAC's output factors.
2. Determine the thermoplastic percentage depth dose and thermoplastic factor.
3. Determine the skin dose and the dose at maximum depth (D_{max}), and also the effects of the thermoplastic mask on them.
4. Use an anthropomorphic phantom for dose verification.
5. Make appropriate recommendations from the findings.

1.4 Relevance and Justification

Since the primary aim of radiotherapy is to accurately and precisely deliver a prescribed dose to a target volume while sparing surrounding healthy and critical tissues, the dosimetric effect of certain treatment parameters must not be overlooked in today's radiation therapy.

In radiotherapy, the accurate and precise delivery of radiation doses critically depends on the day-to-day reproducibility of patient positioning. Now, different immobilization devices are available to help in providing precise repositioning during radiation treatments and also increasing patient comfort. Thermoplastic masks are widely used in head and neck cancer treatments because cancer in the head and neck areas are in close proximity to critical organs and it is required that patients are properly immobilized in order to achieve the goals of immobilization devices.

During simulations or treatments, lasers are used in aligning the patient in the room and these thermoplastic masks provide suitable space for the use of fiducial markers which eliminates the markings on the skin (face) of the patient. On the contrary, the presence of these immobilizing devices (thermoplastic masks) have the tendency of attenuating part of the radiation beam and further increasing skin and build-up region doses which could change the intended plan. For that reason, understanding how these devices affect skin and the build-up region doses in a particular treatment form is of great importance. This would ensure that medical physicists consider their effects and hence make appropriate setup corrections and other adjustments (that is, firmly stretching the mask to reduce its thickness) to keep acceptable doses to skin and build-up regions.

1.5 Scope and Limitation

Some works have been done to investigate skin and build-up region doses in radiotherapy using various methods. However, this study focuses on employing the application of thermoplastic masks as the immobilization device stretched at three different lengths in order to obtain different hole diameters (unstretched, 5 cm stretched, and 10 cm stretched) during head and neck cancer treatments with a 6 MV 3D conformal Plan in radiation therapy. This was done at the Sweden Ghana Medical Centre using the medical linear accelerator. The Roos Chamber type 34001 and the GafChromic EBT3 films are used in this study because they are user-friendly and can easily be used to measure the surface dose whiles on the other hand, the Farmer type Ion Chamber cannot be used to measure the surface dose directly but can only be determined from the PDD. Measurements are made in a solid water phantom at the surface (skin), the build-up region, the d_{max} = 1.6 cm and a specified depth of 10 cm for the 6 MV photon beam at field sizes of 5 x 5, 10 x 10, 15 x 15, and 20 x 20 cm^2.

1.6 Organization of Thesis

This study is arranged in a chronological order of five chapters. Chapter One introduces the research of which comprises; the background of the study, problem statement, objectives, relevance, and justification, scope and limitation. Chapter Two reviews existing literature relevant to the research problem. Chapter Three focuses on the materials and methodologies used for the study. Chapter Four presents the results obtained and discussions performed. Chapter Five is the conclusion of the study and recommendations made from the study.

CHAPTER TWO

LITERATURE REVIEW

2.1 Introduction

Surface dose varies quite significantly using megavoltage radiations in clinical radiotherapy. These differences can be ascribed to variations in electron contamination and phantom scatter (Alnawaf et al., 2012). Majority of these discrepancies are detected for fluctuations in some beam parameters such as use of beam modifying devices, field size and the radiation beam angle of incidence (Hounsell & Wilkinson, 1999; M. J. Butson et al., 1996) or due to the composition of the material which may be in the direct or indirect path of the radiation beam in question (Martin J. Butson et al., 2007).

During external beam radiation therapy, the skin is mostly in danger from radiation effects such as skin shedding, necrosis, and erythema. Epidemiological studies have also found a link between basal cell carcinoma and radiotherapy (Kry et al., 2012). However, skin dose is complicated because of the different skin layers with various depths of thickness that varies between patients and positions on the patient. Besides, the International Commission on Radiological Protection (ICRP) recommends measuring the radiation dose to the skin at 0.07 mm (ICRP, 1977; ICRU, 1985) and 1.0 mm (M. Butson et al., 1997) depth for the basal layer which is taken as the surface dose and dermal layer respectively. (Court et al., 2008); (Dogan & Glasgow, 2003); (Panettieri et al., 2009) have indicated that even though the surface dose may be evaluated with the TPS, mostly within ± 25% accuracy, this method requires computed tomography images and an estimated treatment plan. (Lamb & Blake, 1998) in their studies proposed a skin dose estimation technique on the beams central axis as a function of the treatment parameters.

Nevertheless, their model evaluated only 6 MV and 10 MV photon beams and it is limited to the central axis of the radiation beam.

2.2 Skin and Buildup Region Doses

When a patient is undergoing radiation therapy with a high energy photon, the surface dose is said to be significantly lower than the radiation dose at the d_{max} that occurs in the subcutaneous tissues. Notwithstanding the rise in extreme ionization at or close to the skin as a result of the lower-energy beams, the megavoltage or high energy photon beams produce an initial electronic build-up with depth. Consequently, the skin dose is less than that at d_{max} which occurs at a depth downstream. Research has shown that the higher the radiation energy, the deeper the penetration power and the d_{max}. (F. M. Khan, 2014) stated that "for a higher energy photon beams, dose in the build-up region results from the relatively long range of energetic secondary charged particles (positive and negative) that are first released in the patient by photon interactions and then deposit their kinetic energy in the patient". The low skin dose is known as the skin-sparing effect, which is mostly absent in superficial or orthovoltage beams. This effect, which is a property of megavoltage beams may be reduced or even lost if the radiation beam is extremely contaminated with secondary electrons. Orthovoltage and superficial beams do not demonstration skin-sparing effects given that the maximum dose transpires at the patient's skin surface. Immediately under the patient's skin surface, the condition of charged particle equilibrium (CPE) ceases to exist and the absorbed radiation dose is thus much smaller than the collisional kerma. However, with increasing depth in the patient, the charged particle equilibrium is finally reached at $d = d_{max}$ where d is nearly equal to

the range of the secondary charged particles and the radiation dose becomes comparable with the collisional kerma. Beyond d = d_{max}, both collisional kerma and absorbed dose decreases due to photon attenuations in the patient that results in transient rather than true CPE (Podgorsak & Rosenberg, 2005).

2.2.1 Electron Contamination of Photon Beams

The surface dose in megavoltage photon beams is predominantly due to the contamination of electrons in the incident radiation beam in conjunction with the backscattered ionizing radiation (both electrons and photons) from the material medium.

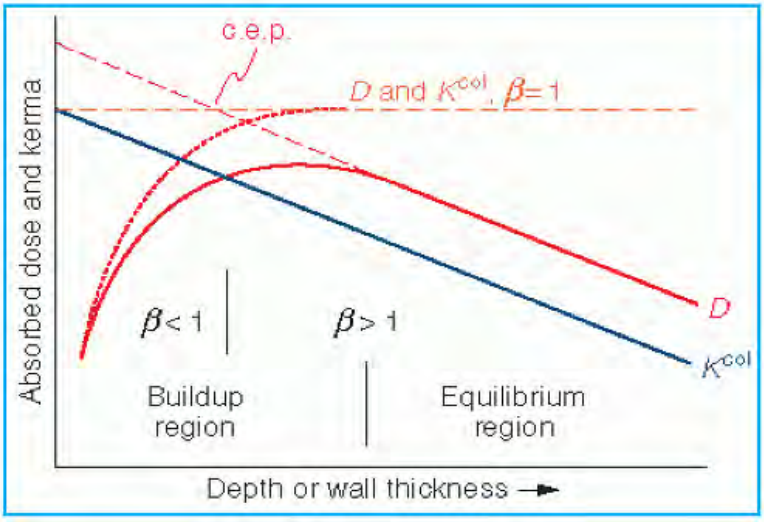

Figure 2. 1: A graph of absorbed dose and kerma as functions of depth

(Biggs & Ling, 1979); (Padikal & Deye, 1978) indicated that electrons were the cause of the increased dose. On the other hand, other researchers in (Biggs & Ling, 1979) iterated that for the Clinac-35 linear accelerator (Varian Corporation, Palo Alto, California), the additional dose in the build-up region is as a consequence of electrons, photons or both. However, no attempts were made to clarify the relative importance of each entity. The depth dose characteristics of a 34 MV photon beam from an Asklepitron 45 (a 45 MeV

betatron) was studied by Dawson (Biggs & Ling, 1979) and drew a conclusion that electrons were the greatest contributor. Also, (Marbach & Almond, 1977) in their publication postulated that for a 25 MV radiation beam from a Sagittaire, Compton scattered photons were the cause for the added dose in the build-up region. Studies have shown that virtually all X-ray and gamma-ray beams employed in radiotherapy mostly face contamination with secondary electrons (mostly Compton electrons) produced by the photon interactions with the collimator, air, the flattening filter, and other materials in the path of the beam such as wedges and shadow tray. Electron contamination also disturbs the disparity of dose in the build-up region with field size. (Dogan & Glasgow 2003) described a decreased build-up region dose when comparing IMRT strip fields to open beam fields and established that any rise in skin toxicity was not inherently due to IMRT delivery techniques. (Biggs & Ling, 1979); (F. M. Khan, 2014) stated that "as the field size increases, the depth dose in the build-up region increases, resulting in a shift in the depth of maximum dose, d_{max}, to increasingly shallower depths". Researchers such as (Biggs & Ling, 1979); (Marbach & Almond, 1977); (Padikal & Deye, 1978) have shown that this effect is mainly triggered by the secondary electrons.

2.2.2 Skin-Sparing Effect as A Function of Photon Energy

Researchers have indicated that the dose distribution in the build-up region relies on numerous variables such as SSD, field size, photon beam energy, and configuration of the secondary blocking trays (F. M. Khan, 1971; Pillai et al., 1973; Velkley et al., 1975). Certain studies have indicated that there is a reduction in skin dose at higher photon beam energies (Martin J. Butson et al., 1998; Chiu-Tsao & Chan, 2009; Lin et al., 2001;

Stathakis et al., 2006). However, other studies provide contrary view, particularly for large field sizes (M. Butson et al., 1997; De Ost et al., 1997; Kim et al., 1998; Klein & Purdy, 1993; Yu et al., 2003) as demonstrated with lower energies (6-10 MV) and higher energies (15-18 MV). Nevertheless, Cobalt-60 is said to create a higher skin dose which further increases with field size and ranged between 20% - 85% of d_{max} for the open beam (Kry et al., 2012). Though the skin-sparing effect relies on many conditions, the outcome, in general, becomes well pronounced as the photon energy increases. (Martin J. Butson et al., 1998) in their studies on the central axis of the photon beam relative to d_{max} for a field size of 10 x 10 cm^2 and obtained measured skin doses greater by 22%, 17%, and 15.5% corresponding to 6, 10, and 18 MV respectively.

Table 2. 1: Buildup Dose Distribution in Polystyrene for a 10 × 10 cm^2 Field

Depth (mm)	^{60}Co 80 cm[a] (cGy)	4 MV 80 cm[a] (cGy)	10 MV 100 cm[b] (cGy)	25 MV 100 cm[a] (cGy)
0	18.0	14.0	12.0	17.0
1	70.5	57.0	30.0	28.0
2	90.0	74.0	46.0	39.5
3	98.0	84.0	55.0	47.0
4	100.0	90.0	63.0	54.5
5	100.0	94.0	72.0	60.5
6	-	96.5	76.0	66.0
8	-	99.5	84.0	73.0
10	-	100.0	91.0	79.0
15	-	-	97.0	88.5
20	-	-	98.0	95.0
25	-	-	100.0	99.0
30	-	-	-	100.0

[a]Data from Velkley et al., (1975)

[b]Data from F. Khan, Moore, & Levitt, (1973)

2.2.3 Effects of Thermoplastic Immobilizers on Surface Dose.

Thermoplastic immobilization devices are mostly used worldwide in head and neck radiation therapy to substantially improve the precision of treatment delivery. However, there have been concerns regarding the rise in radiation-induced skin morbidity with the use of these devices thereby eliminating the skin sparing effect of megavoltage radiation (Fiorino et al., 1992; Mellenberg, 1995). (Hadley et al., 2004) reported that a rise in surface dose from 16 to 27% for a 6 MV megavoltage radiation was observed when thermoplastic masks were used, however, this may increase the skin toxicity and can be detrimental for the patient's quality of life. (Mellenberg, 1995) in his studies observed that, for 6 and 15 MV photon energies, the PDD measured at the surface just behind the used thermoplastic mask was 35.7% and 24.3% respectively which agrees well with the PDD measured at 0.6 mm in the beam without the thermoplastic mask (33.8% and 24.5%). In conclusion, he noted that surface dose increases as a gram per square centimeter relationship for thermoplastic masks. In 2002, research was conducted to determine the cause of acute skin toxicity in head and neck cancer treatment with extended-field intensity-modulated radiotherapy by (Lee et al., 2002). They observed that the estimated surface dose with the thermoplastic mask was constantly larger than those without the thermoplastic mask. An average rise in dose of approximately 18% was estimated which was ascribed to the bolus effect of the masks used for IMRT treatment. Lee et al. later reported that measurements on a phantom presented that the mask had a "bolus" effect on the surface of the skin and at the same time did not take the skin into consideration as one of the sensitive structures during treatment planning. They also added that the use of multiple tangential fields in intensity-modulated radiation therapy

plans contributes to an increase in surface dose by approximately 19% and 27% with and without the thermoplastic mask, respectively. In conclusion, they suggested the skin should be taken into consideration as one of the sensitive structures during treatment planning and to reduce the "bolus" effect of the thermoplastic mask was to stretch hard on the mask to "thin" it out as shown in figures 2.3 – 2.5. (Higgins et al., 2001) in their studies measured a rise in skin dose as a result of the carbon fiber tables used and it was as high as 400%. They reported that the presence of the carbon fiber substantially reduced the skin-sparing effect by a magnitude which was relatively larger for small beam sizes. They concluded from their research that, the skin dose was approximately four times as large when the carbon fiber was added to the 10 x 10 beam and approximately double for the 40 x 40 beam. Works have been done by Hadley et al. (2004) to investigate the rise in skin dose triggered by the use of thermoplastic mask and quantify the change between the mask samples presented. The solid water phantom in conjunction with the Attix parallel plate chamber was used to determine the change in the dose build-up by measuring the tissue maximum ratios (TMRs). Using dual energies of 6 and 15 MV, measurements were obtained with and without the thermoplastic mask on top (surface) of the solid water phantom and the effective thickness of equivalent water was estimated from the TMR curves. They measured the build-up effect to be equivalent to 0.6 to 2.2 mm for the thermoplastic masks that have been extended at varying hole diameters. The increase in skin dose was projected to rise from 16% and 12% for 6 MV and 15 MV respectively to 27% to 61% for 6 MV and 18% to 40% for 15 MV with the thermoplastic mask samples. Below are sample images of thermoplastic masks with

figure 2.6 showing the physical effect of the thermoplastic mask on patient's skin during a radiation therapy treatment.

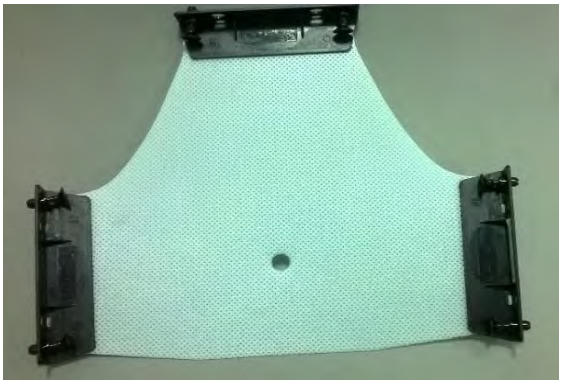

Figure 2. 2: An unstretched thermoplastic mask

Figure 2. 3: A stretched thermoplastic mask to be used on the solid water phantom

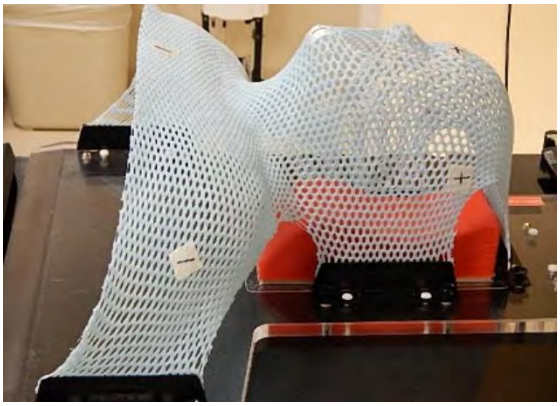

Figure 2. 4: A thermoplastic mask fixed to the couch in the treatment room

Figure 2. 5: A moulded thermoplastic mask during simulation

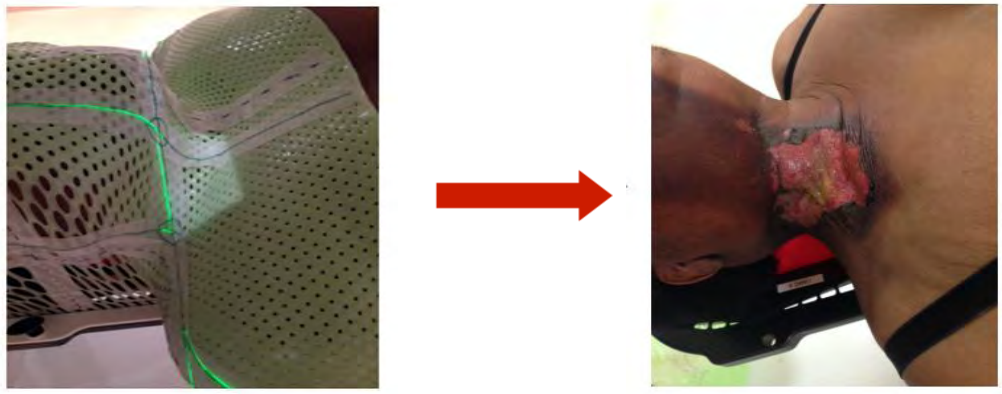

Figure 2. 6: The effect of thermoplastic mask on skin dose

2.2.4 Effect of Field Size on Skin/Surface Dose

(Yadav et al., 2009) studied surface dose estimations for numerous beam modifiers at different SSD's for 6 MV photon beam using an acrylic slab phantom and a Markus 0.055 cc parallel plate ion chamber to measure the skin and build-up region doses. They undertook measurements for motorized wedges, open fields and acrylic block tray fields for various field sizes of 3 x 3 cm^2 to 30 x 30 cm^2. They later concluded from their research that the skin dose for all the beam modifiers increased with increasing field size. Considering the block trays, they indicated that electrons were eliminated from the upstream but generated its own new secondary electrons increasing the number of electrons generated upstream as compared to the ones removed downstream by the tray, thereby increasing the surface dose. For the 60^o motorized wedge fields, they realized that, at larger field sizes, the increase in skin dose was higher as compared to that for the open fields. For the physical wedges, electrons were eliminated from upstream and were produced by itself; with the number generated being less than the ones eliminated for smaller field size (Kry et al., 2012; Yadav et al., 2009). Increasing field size generally comes with increasing surface dose which is as a result of the higher electron emissions from the collimator and air (F. M. Khan, 2014). Figure 2.7 below is a graph showing relative skin dose against field size for Co-60, 4 MV, and 10 MV photon beams. These data indicate that the skin-sparing effect is substantially lowered for the higher field sizes.

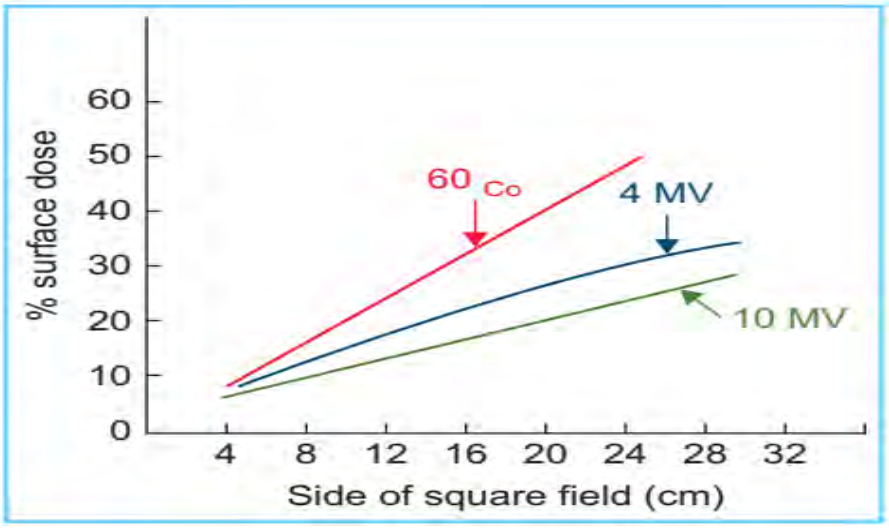

Figure 2. 7: Percentage skin dose against field size. (Data from Velkley, et al., 10 MV data are from Khan FM, et al.)

2.3 Exit Dose

Research has shown that in megavoltage X-rays, the radiation exit dose is influenced by the dose build-down due to the missing backscatter material beyond the patient's exit surface (Kron & Ostwald, 1995). Kron and Ostwald stated that "since the build-down effect is typically less pronounced as the build-up effect at the entrance portal of the X-ray beam, the exit dose may contribute significantly to the skin dose and to a possible unwanted skin reaction". It is usually complicated to measure the exit dose than the entrance dose. However, in the absence of the backscatter material, the skin dose is less than predicted by PDD by approximately 15% (relative difference) for 6 MV or Co-60 beams and is not mostly different for other higher beam energies (Gagnon & Horton, 1979; Klein & Purdy, 1993; Purdy, 1986; Stathakis et al., 2006). Although full scatter conditions are attained (as predicted by the percentage depth dose) with minimal material, as well as virtually any immobilizing device behind the patient (Gagnon & Horton, 1979; Klein & Purdy, 1993; Purdy, 1986).

2.4 Radiation Dosimeters for Skin Dose Measurements

A device, tool or a system that is used in measuring or evaluating either indirectly or directly: absorbed dose, equivalent dose, kerma, exposure or associated quantities of ionizing radiation is known as a radiation dosimeter. It can provide a measurement that is a degree of the average absorbed dose deposited in its sensitive volume by the radiation. It is referred to as a dosimetry system in conjunction with its reader. For a device to work as a dosimeter, it must have at least one physical characteristic that is dependent on the measured quantity and that can be used for measuring the radiation with correct calibration. Nevertheless, to be suitable, the dosimeters must show various required features. For instance, the dimensions of the dosimeter should be as small as possible along the incident beam, due to the steep dose gradient in the build-up region. Hence, an extrapolation chambers is the suitable instruments for such the measurements as indicated by (Khan, 2014). However, only a few centers have these radiation dosimeters available and as an alternative, the fixed plane-parallel ion chambers are usually used for this purpose. In addition to ionization chambers, thin layers (< 0.5 mm) of TLD material (Rapley, 2006) and radiochromic films such as the GafChromic films are available for measurements of skin dose. The film is first calibrated within the dose range required before use (Butson et al., 1999; Khan, 2014). In this study, the choice of the ionization chamber and GafChromic films were made due to its availability at the facility.

2.4.1 Ionization Chambers

Ionization chambers are types of radiation dosimeters which are employed in both radiation therapy and diagnostic radiology for the measurement of doses. They come in

numerous sizes and shapes subject to a particular requirement, but usually they possess these features: It is fundamentally a gas-filled cavity that is enclosed by a conducting outer layer with a collecting electrode at the center which is separated with a high-quality insulator in order to decrease the leakage current when a polarizing voltage is applied to the chamber. Additional chamber leakage is reduced by means of a guard electrode that cuts off the leakage current and permits it to move to the ground, avoiding the collecting electrode. Better charge collection due to enhanced field consistency in the sensitive/active volume of the chamber is another advantage. However, (Podgorsak & Rosenberg, 2005) stated that temperature and pressure corrections are required during measurements with open-air ion chambers to help explain the variation in air density in the chamber volume as a result of a change in ambient temperature and pressure. Particularly, for skin dose measurements are the fixed plate ionization chambers and the extrapolation chambers (Andreo et al., 1995; Khan, 2014; Rawlinson et al., 1992). In this work, a Roos Chamber type 34001, used for dose or dose rate measurement for the measuring quantity "absorbed dose to water" in solid water phantoms and used for the determination of relative depth dose curves of megavoltage beams was used in conjunction with an electrometer. The Roos chamber is said to be waterproof, fully guarded having a 15 mm width collector and a nominal sensitive volume of 0.35 cm^3.

2.4.2 Electrometers

Electrometers are devices used for measuring small currents (approximately $\leq 10^{-9}$ A). When used in combination with an ion chamber, it gives a high gain, negative feedback,

operational amplifier with a standard resistor or a standard capacitor in the feedback path to determine the ion chamber current or charges collected over a time range.

2.4.3 Radiochromic Film

Several methods and procedures have been developed for the measurement of a patient's skin dose using different dosimeters. This research seeks to use a new type of film in radiotherapy dosimetry known as the radiochromic film. GafChromic films are said to be the most commonly used films in dosimetry (e.g. HD-810 film, DM-1260, EBT, EBT2, EBT3, MD-55 and MD-55-2 film with an effective depth of skin dose measurement at 0.17mm ± 0.03mm). They are said to be colourless films with closely tissue equivalent composition (11.2% nitrogen, 19.2% oxygen, 60.6% carbon, and 9.0% hydrogen) which changes colour to dark blue upon radiation exposure. The unexposed radiochromic film is said to be colourless and changes colour to shades of blue due to its composition of a special dye that polymerizes as a result of its interaction with radiation. After the absorption of light by the polymer, the light transmission through the radiochromic film can be measured using an appropriate device known as a densitometer. Radiochromic film requires no chemical, physical or thermal processing to bring out or stabilize this colour. Studies have shown that the film's ability to respond to radiation exposures less than 50 mGy is not noticeable making the flatbed scanner incapable of picking up the small changes in film color (Lewis, 2009). Radiochromic films used in dosimetry is said to have some potentials over radiographic films such as ease of use; eliminates the need for darkrooms, film cassettes or film processing (chemicals); insensitive to ambient conditions and improved energy characteristics making it useful at higher doses

(Podgorsak & Rosenberg, 2005). Radiochromic films are relative dosimeters and must be well calibrated before used for dosimetry, however, with proper calibration and taking into account the environmental conditions, a precision better than 3% can be archived (Khan, 2014). The film is also used for field size alignment and shaping of radiation fields, detecting radiation leakage around the collimator head and positioning of special radiation fields (Niroomand-Rad et al., 1998). With careful handling and calibration of the film in accordance with the overall recommendations outlined by the manufacturer's specifications as stated in the AAPM TG-55 report by (Niroomand-Rad et al., 1998) it should be possible to achieve a precision of better than 3% for dosimetric work.

2.4.3.1 Introduction

A GafChromic [International Specialty Products (ISP), Wayne, NJ] EBT3 film which is specifically developed to address the need of a medical physicist working in the radiotherapy setting and a type of a radiochromic film was used for this study. The active range of the film is constructed for greatest operation in the dose range from 0.2 to 10 Gy. This makes it good for various applications in intensity modulated radiotherapy (IMRT), VMAT and brachytherapy. Like the previous versions, EBT3 is said to be self-developing, requiring neither developer nor fixer. Some of the main technical features of the GafChromic EBT3 film include:

It is a near tissue equivalent material which requires no post-exposure treatments since it develops in real time. It has a dynamic dose range of 0.1 to 20 Gy with 0.2 to 10 Gy being its optimum dose range although it has a slight response variation from 100 keV into the MV range. The film has a high spatial resolution, hence, can resolve features

down to 25 µm or less. It is water-resistant and usable with water phantoms with a new technology of incorporating a marker dye in its active layer to decrease UV/visible light sensitivity and also enable using multi-channel dosimetry for non-uniformity correction. The film is said to be stable at temperatures up to 60^0C.

2.4.3.2 Configuration and Structure of GafChromic EBT3

The structure of the GafChromic EBT3 film is shown in figure 2.8 below. The EBT3 film is made up of an active layer, nominally 28 µm thick, sandwiched between two 125 µm matte-polyester substrates. This active layer comprises a marker dye, the active component, stabilizers and other components giving the film its close energy independent response. The thickness of the active layer will differ to some extent between different production lots.

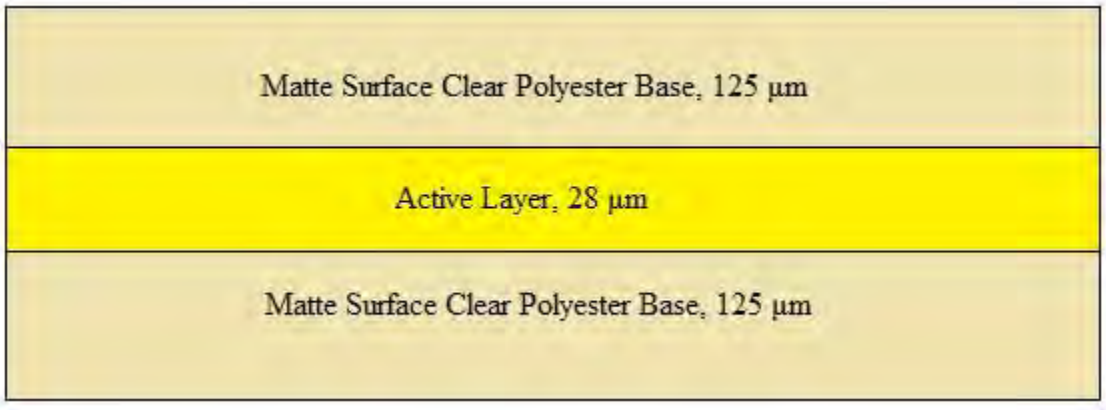

Figure 2. 8: Structure of GafChromic EBT3 Dosimetry Film (Actual thickness may vary slightly).

(Sipilä et al., 2016) in their studies indicated that "the surface of the radiochromic film is covered with tiny silicone spheres eliminating Newton's rings artifact in the image". Further explanation of the film feature is described by (David Lewis et al., 2012) in their research.

2.4.3.3 Medical Applications

Radiochromic films are said to be comparatively unresponsive to ionizing radiation compared to frequently used detectors in medical applications making it ideal for dosimetry where high radiation doses are applied (Niroomand-Rad et al., 1998). The application of radiochromic film in the medical fields is vastly extending from high-dose gamma ray exposures in brachytherapy to low-dose clinical valuation in-vivo such as conventional radiation therapy of breast cancer patients. Below are three medical applications of a GafChromic (radiochromic) films (Martin J. B. et al., 1999; Stevens et al., 1996).

i. Proton Dosimetry

(Nichiporov et al., 1995; Vatnitsky, 1997 and Vatnitsky et al., 1997) indicated that one of the useful detectors in clinical proton beams for dosimetry measurements is the radiochromic films. It possesses a fundamental composition equivalent to that of water, which decreases its sensitivity to photon energy for an application dealing with the determination of dose delivered to water as is given in TG-55 (Niroomand-Rad et al., 1998).

ii. Skin and Surface Dosimetry

Due to the low energy reliance of the film, relatively small effective thickness and the ability to produce a two-dimensional dose map which other skin dosimeters in radiotherapy is currently lacking, the radiochromic film is a detector for choice. These applications include in-vivo dosimetry as well as phantom studies for dose calculation at

the skin surface, dermal and basal cell layers as well as the subcutaneous layers as indicated by (Niroomand-Rad et al., 1998).

iii. Brachytherapy

In brachytherapy, one of the advantages is the sharp or steep dose fall-off outside the tumor or target volume. From the inverse square law, radiation dose at a point close to the radiation source can be very high, which becomes a problem with the use of conventional detectors. The low sensitivity and high resolution of the radiochromic film give it an advantage over the other detectors which makes it useful for dosimetry near these high activity sources (Niroomand-Rad et al., 1998).

2.4.3.4 Advantages of GafChromic Films

Below are some of the advantages of using GafChromic films for dosimetry.

The GafChromic film gives permanent absolute values of absorbed dose with a satisfactory accuracy and precision. It provides a larger area for dosimetry; including beam profiles. It has a higher spatial resolution and easy to handle and analyze. Non-uniformity correction is possible when using multi-channel dosimetry. The film is water-resistant and usable with water phantoms. It needs no darkrooms, film processing (chemicals) or cassettes due to its real-time developments without post-exposure treatment. The film is said to be insensitive to visible light.

CHAPTER THREE

MATERIALS AND METHODS

The methodologies adopted to assess the effects of thermoplastic immobilization mask on patient's skin and the build-up region doses in the head and neck region for high energy photon beams using a Roos Chamber type 34001 coupled with PTW Freiburg UNIDOS Electrometer and EBT3 GafChromic films for different field sizes are presented in this chapter. Known procedures for the calibration of GafChromic EBT3 films for assessing skin dose with solid water phantom together with the dose measurements are outlined in this chapter.

3.1 Materials

The materials used in this study include; a medical linear accelerator unit (figure 3.1), anthropomorphic phantom, plastic water (PMMA) phantom, PTW Freiburg UNIDOS electrometer, Roos chamber type 34001, thermoplastic masks, EBT3 GafChromic film, EPSON STYLUS CX5900 flatbed scanner, water bath, diode, diode reader, digital thermometer, and barometer. Some specific materials are presented with details below.

3.1.1 Medical Linear Accelerator

This is a device most commonly used for the treatment of cancer with external beam radiation. The linear accelerator can be used to treat all body parts or organs of a patient undergoing radiation therapy treatment. The device uses high radio-frequency (RF) electromagnetic waves to accelerate charged particles (electrons) to interact with a heavy metal target and because of these collisions, high energy X-rays (photons) are emitted

from the target in a linear path, within a tube-like structure called the accelerator waveguide. The LINAC delivers these high energy X-rays or electrons to the target tumor as they exit the tube. These treatments can be planned in such a way that they destroy the cancerous cells while sparing the neighboring healthy tissues, thus achieving the desired therapeutic ratio. At Sweden Ghana Medical Centre, there is one Elekta Synergy platform linear accelerator unit in the radiotherapy department. The LINAC delivers both electron and photon energies. It produces two different photon energies (that is, 6 MV and 15 MV) and three different electron energies (that is, 6 MeV, 10 MeV, and 15 MeV) respectively. A specialized multi-leaf collimator of 2 x 40 leaf's and 1 cm leaf width is incorporated in the treatment head at the isocenter. The LINAC is used in treating all body sites, using Intensity-Modulated Radiation Therapy (IMRT), Conventional Techniques, Volumetric Modulated Arc Therapy (VMAT), and Stereotactic Radiosurgery (SRS). The treatment couch used at the Sweden Ghana Medical Center is the precise and hexapod type. Figure 3.1 shows a pictorial view of the Synergy Platform Linear Accelerator unit at SGMC.

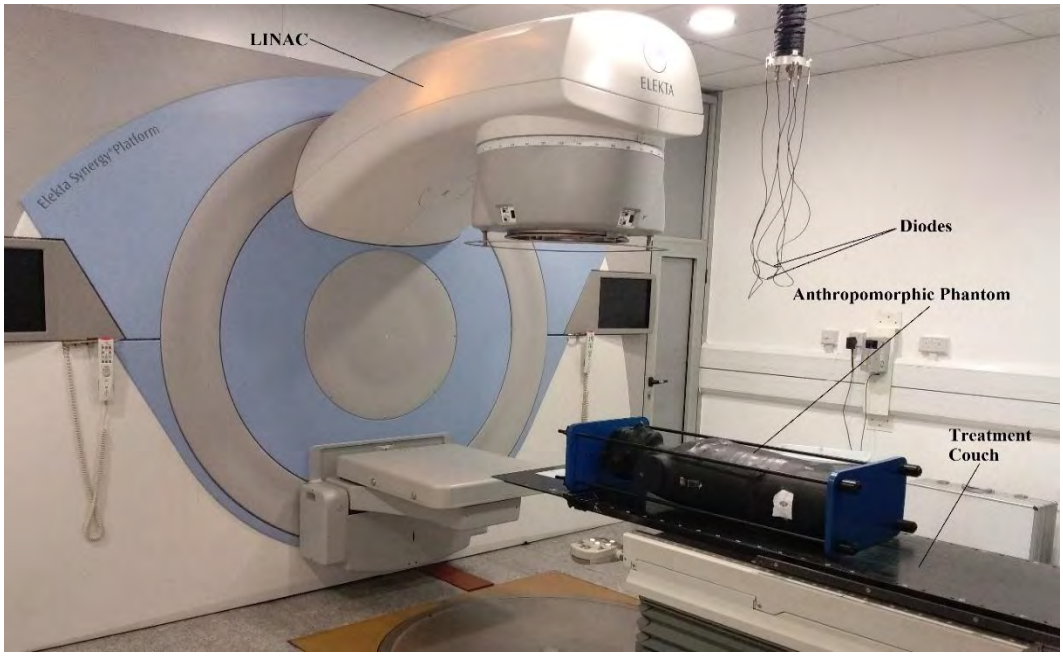

Figure 3. 1: Medical Linear Accelerator at Sweden Ghana Medical Centre (SGMC)

3.1.2 Ionization Chamber

The type of ion chamber used for this study was the Roos type chamber 34001 which is a vented plane-parallel ionization chamber for connection to precision electrometers according to IEC 60731 for measurements in electron beams. It is used as reference chamber in absolute dosimetry, that is, in radiation therapy, the Roos chamber is used for dose or dose rate measurement for the measuring quantity 'absorbed dose to water' in solid state phantoms or water phantoms. The detector has a wide guard ring, which excludes any perturbation effect even at low electron energies and in the build-up range of photon beams. The electron energy response of the detector in the range of 2 MeV to 45 MeV is provided by the stopping power correction. The Roos type chamber requires no corrections due to its design. The Roos chamber as shown in figure 3.2 can also be used for measuring the relative depth dose curves of high energy photon beams. The

Roos chamber is waterproof, fully guarded, has a 15 mm diameter collector, with a supposed sensitive volume of 0.35 cm^3.

Figure 3. 2: Roos Chamber type 34001

Using the Roos Ionization Chamber

The ion chamber was connected to the electrometer and switched on. The high voltage was correctly adjusted on the electrometer and allowed for about 15 minutes to stabilize before the measurements were started. The correction factor for air density was noted and used to correct for the measured values. Lastly, a zero adjustment was performed followed by the measurements.

Application in the Solid Water Phantom

Special chamber plates are available for measurements with the detector in a slab phantom. The chamber plates are available in the form of twin plates. The active point of measurement (reference point) of the detector in this plate is approximately 1 mm below the surface of the twin plate.

Inserting the Detector into the twin plate

The detector is inserted into the twin plate so that the 'crosshairs' is visible and points towards the radiation source as in figure 3.3. Figure 3.4 also shows the final stage of inserting the detector into the twin plate which is placed on the treatment couch for measurements.

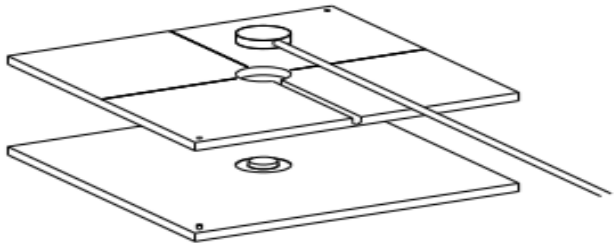

Figure 3. 3: Inserting/removing the Roos Chamber

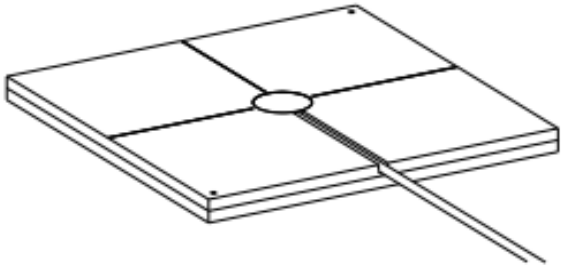

Figure 3. 4: Twin plate with inserted Roos chamber

Removing the Detector from the Twin Plate

To remove the Roos Chamber after measurements, the plate is lifted with the 'crosshairs' and the detector is carefully removed (refer to figure 3.3).

3.1.3 Electrometer

The electrometer used was the UNIDOS (PTW, Freiburg, Germany) model with serial number 000820. Figure 3.5 provides an image of the front view of the electrometer. The

electrometer was calibrated together with the ion chamber mentioned above. It was used to quantify the charges that have been collected by the ionization chamber in nC/minute and the measured values were then corrected for temperature and pressure variations respectively.

Figure 3. 5: PTW UNIDOS Electrometer

3.1.4 Diodes

Diodes are inexpensive, rugged and easy to use as they require no bias. Although they are smaller in size as compared to other ion chambers, diodes are preferred for clinical dosimetry due to its higher relative sensitivity and quick response (1 – 10 μs). However, diodes are said to suffer radiation damage, so they require occasional recalibration. The diodes in this work were used to measure doses at the skin surface and d_{max} in "real time" and recorded accordingly (figure 3.6).

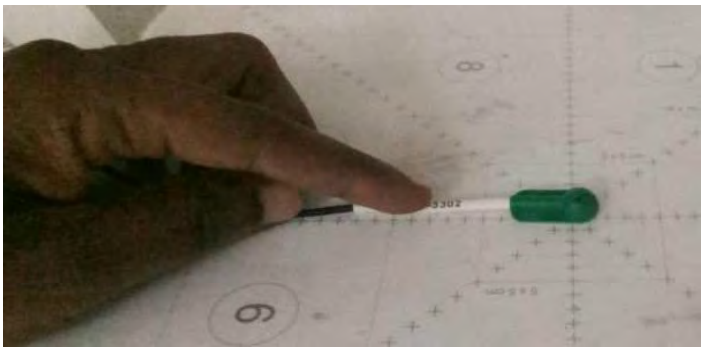

Figure 3. 6: Diode

3.1.5 Water Bath

To make a thermoplastic mask pliable or moldable to obtain the contours of the patient's anatomy, the mask is first placed in a water bath above a specific temperature to make it soft and solidifies upon cooling after molding. The water bath shown in figure 3.7 can modulate/regulate the temperature of the water.

Figure 3. 7: Water Bath

3.1.5 Thermoplastic Immobilization Mask

A thermoplastic mask is a plastic material made up of two parts; a sheet of thermoplastic material and a rigid frame at the edge. When immersed in warm water above a temperature, the mask becomes soft and pliable, after which it is placed over the patient and moulded to the patient surface. As the mask cools down, a rigid replication of the patient's anatomy is formed. The masks were attached to a rigid frame which mounts to the treatment couch. Thermoplastic masks are available commercially to immobilize different patient's treatment sites. In this research, the surface dose was measured with and without the head and neck mask. The masks used in this study were placed on the phantom setup to cover the surfaces.

3.1.6 GafChromic Films

The radiochromic film used here was a GafChromic EBT3 film (lot # 04201601), with known dimensions of 8" x 10". In view of the procedures stated in the AAPM TG-55 report by (Niroomand-Rad et al., 1998), the film was handled and used in accordance with the overall recommendations outlined by the manufacturer's specifications in order to preserve its integrity. (Podgorsak & Rosenberg, 2005) described GafChromic film as a colourless film with nearly tissue equivalent composition that develops a dark blue colour upon its exposure to radiation and it is intended for the determination of absorbed doses of ionizing radiation with a dynamic range intended for greatest operation in the dose range from 0.2 Gy to 10 Gy, making it appropriate for different applications in IMRT, VMAT, and Brachytherapy. It has the ability of self-developing right after exposure and requires neither a developer nor a fixer. During the estimation of doses considerably larger than 10 Gy, EBTXD or MDV3 are chosen while the measurement of still higher dose uses the HDV2.

3.1.7 ImageJ Software

The ImageJ software is a freely available Java-based image processing and analysis software developed/established at the National Institutes of Health (NIH). This software was built with an open architecture that offers extensibility via Java plugins and recordable macros (Girish, V., Vijayalakshmi, 2004) by using objective physical characteristics of the imaging system such as spatial resolution, contrast, and noise. The user-written plugins make it possible to solve almost any image processing and analysis

problems (Eliceiri & Rueden, 2005). Figure 3.8 shows the interface of the ImageJ software.

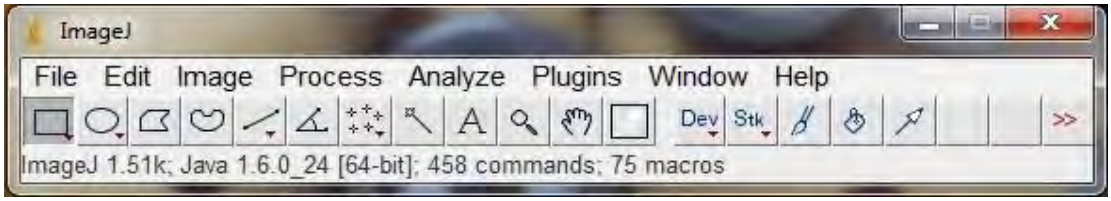

Figure 3. 8: Image J software interface

3.1.8 Other Materials

Figure 3.9, 3.10, 3.11, and 3.12 are images of a barometer, diode reader, solid water phantom with known dimensions of 30 x 30 cm^2, and a thermometer respectively, which were used for the setup.

Figure 3. 9: Barometer

Figure 3. 10: Diode reader

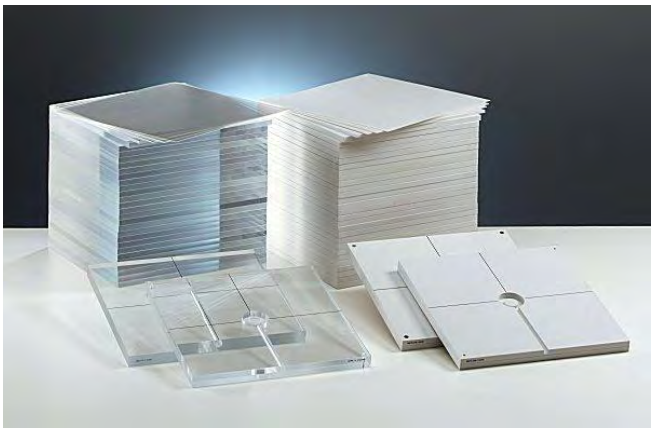

Figure 3. 11: Solid water phantom

Figure 3. 12: Thermometer

3.2 Experimental Method

In radiotherapy, before any measurement is clinically done, it is required that thorough quality control tests are performed. These tests were performed on all equipment before any measurement was taken, and all the equipment were allowed to acclimatize to the room's conditions. The chamber was pre-irradiated for about 5 minutes to remove all traces of stray charges and checked for stability. The solid water phantom was setup on the LINAC's couch, perpendicular to the beams central axis using the isocentric technique. The Roos chamber was positioned, coupled with the UNIDOS electrometer at the required depth within the phantom and used to collect and measure the charges respectively. The initial temperature and pressure were recorded using the thermometer and the barometer respectively.

3.2.1 Part 1:

3.2.1.1 Measurement Without Thermoplastic Mask

Using a varying field size of 5 x 5, 10 x 10, 15 x 15, and 20 x 20 cm^2 without a thermoplastic mask as illustrated in figure 3.13, the ionization chamber was irradiated with 100 MU (1 Gy) for the open beam. The charges collected by the ion chamber was measured and recorded using the electrometer. Three successive measurements were taken for each field size and their average values estimated and recorded. The final temperature and pressure were recorded using the thermometer and the barometer respectively. The experiment was repeated for other depths of 0, 1.6 (d_{max}), 4, 6, 8, and 10 cm for the open beam. Temperature and pressure correction was performed for all charge measurements.

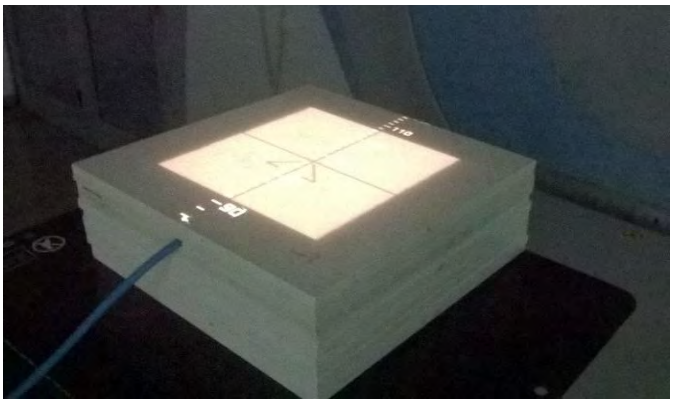

Figure 3. 13: Setup without a thermoplastic mask

3.2.1.2 Measurement on an Unstretched Thermoplastic Mask

Using a varying field size of 5 x 5, 10 x 10, 15 x 15, and 20 x 20 cm^2 with an unstretched mask as illustrated in figure 3.14, the ionization chamber was irradiated with 100 MU (1 Gy) for the open beam. The charges collected by the ion chamber was measured and recorded using the electrometer in charge mode. Three successive measurements were taken for each field size and their average values estimated and recorded. The final temperature and pressure were recorded using the thermometer and the barometer respectively. The experiment was repeated for other depths of 0, 1.6 (d_{max}), 4, 6, 8, and 10 cm for the open beam. Temperature and pressure correction was performed for all charge measurements.

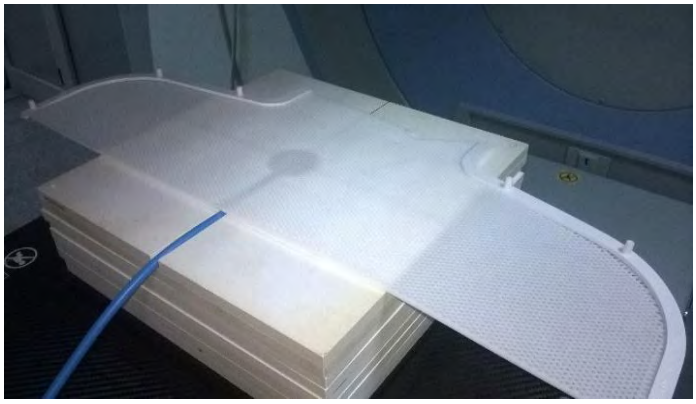

Figure 3. 14: Setup with an unstretched thermoplastic mask

3.2.1.3 Measurement on a 5 cm Stretched Thermoplastic Mask

The thermoplastic mask was placed into a water bath and heated to a temperature of about 70 ^{0}C for about 1 minute. The mask was removed from the water bath, stretched slightly to a length of 5 cm and fixed on the surface of the phantom as shown in figure 3.15 below and allowed to harden for about 5 minutes. Using a varying field size of 5 x 5, 10 x 10, 15 x 15, and 20 x 20 cm^2 with the 5 cm stretched mask, the ion chamber was irradiated with 100 MU (1 Gy) for the open beam. The charges collected by the ion chamber was measured and recorded using the electrometer in charge mode. Three successive measurements were taken for each field size and their average values estimated and recorded. The final temperature and pressure were recorded using the thermometer and the barometer respectively. The experiment was repeated for other depths of 0, 1.6 (d_{max}), 4, 6, 8, and 10 cm for the open beam. Temperature and pressure correction was performed for all charge measurements.

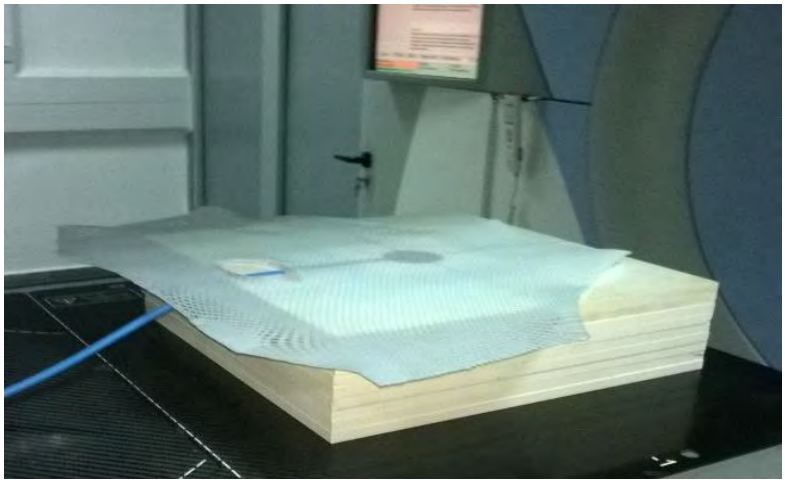

Figure 3. 15: Setup with a 5 cm stretched thermoplastic mask

3.2.1.4 Measurement on a 10 cm Stretched Thermoplastic Mask

The thermoplastic mask was re-immersed into the water bath, removed, stretched fully to a length of 10 cm to obtain a very small thickness. Using a varying field size of 5 x 5, 10 x 10, 15 x 15, and 20 x 20 cm^2 with the 10 cm stretched mask, the ion chamber was irradiated with 100 MU (1 Gy) for the open beam. The charges collected by the ion chamber was measured and recorded using the electrometer in charge mode. Three successive measurements were taken for each field size and their average values estimated and recorded. The final temperature and pressure were recorded using the thermometer and the barometer respectively. The experiment was repeated for other depths of 0, 1.6 (d_{max}), 4, 6, 8, and 10 cm for the open beam. Temperature and pressure correction was performed for all charge measurements.

3.2.1.5 Temperature and Pressure Correction

Since calibration factors are for standard environmental conditions of temperature at T_0 = 22 ^{0}C and P_0 = 110.33 kPa, charge readings were corrected to standard environmental conditions using the equation:

$$\mathbf{P_{PT}} = \frac{(273.2 + T)}{(273.2 + 22.0)} \times \frac{(101.33)}{P} \qquad \text{..... (3.1)}$$

Where T, P, and P_{PT} is the temperature in degrees Celsius, the pressure in kilopascals and the correction factor respectively. The average readings were then multiplied by the correction factor, P_{TP} to acquire the corrected reading:

$$\mathbf{M_{cor} = M \times P_{TP}} \qquad \text{..... (3.2)}$$

Where M is the average ionization chamber reading and M_{cor} is the corrected average ionization chamber reading.

3.2.1.6 Measurement of The Thermoplastic Mask Factor, TF.

To know and correct for the effects the thermoplastic mask has on the skin dose, the thermoplastic factor variation with depth and field size were determined. Just like the tray factor, the thermoplastic mask factor is expressed as a ratio of the corrected ion chamber readings with mask I_1 to that without mask I_0. That is,

$$\mathbf{TF = I_1/I_0} \qquad \ldots\ldots\ldots\ldots\ldots\ldots \quad (3.3)$$

3.2.2 Part 2:

3.2.2.1 GafChromic Film Calibration

A solid water phantom (PTW, Freiburg, Germany) of dimensions 30 x 30 cm^2 was used for the calibration with 10 cm of the build-up material above and below the GafChromic film. The field size of 10 x 10 cm^2 was used at the isocenter and SSD was set at 100 cm. The GafChromic film samples were cut (2 x 3 cm^2) and irradiated perpendicularly to the beams central axis for the 6 MV photon beam. A calibrated ion chamber was introduced in the water phantom below the film level to determine the LINAC's output during the irradiation process and measured the absorbed dose deposited to the film by employing the IAEA-TRS 398 protocol (Musolino, 2000). To acquire a calibration curve, the films were irradiated with the LINAC (using 6 MV) of uniform radiation at dose levels of 0, 0.20 Gy, 0.40 Gy, 0.80 Gy, 1.60 Gy, 2.40 Gy, 3.20 Gy, 4.00 Gy, and 5.00 Gy. The cut films were labeled with respect to the above radiation doses.

3.2.2.2 Measurement of Skin Dose Using GafChromic Films

Skin dose measurements were carried out using GafChromic films. Firstly, the GafChromic film was cut into small pieces with dimensions of 2 x 3 cm^2 each and labeled as A, B, and C respectively. Film A was positioned on top of the phantom, film B at the d_{max} of 1.6 cm for the 6 MV photon beam, and film C placed at a depth of 10 cm as shown in figure 3.16 below. GafChromic film C was used to determine the percentage depth dose (PDD) at a reference depth of 10 cm within the phantom and compared with the PDD at a depth of 10 cm for the LINAC beam. Using the isocentric technique, the labeled films, A, B, and C were placed at the surface, d_{max} and at a reference depth of 10 cm respectively. Using a varying field size of 5 x 5, 10 x 10, 15 x 15, and 20 x 20 cm^2, the films were then irradiated/exposed with 100 MU (1 Gy) for the open beam. For each field sizes, the set of films A, B, and C were kept together in an envelope labeled with the various field sizes.

Figure 3. 16: Positioning of the film set A, B, and C at the surface of the phantom, at the d_{max} of 1.6 cm for the 6 MV photon beam, and at a depth of 10 cm respectively

3.2.2.3 Measurement of Skin Dose with The Introduction of Thermoplastic Immobilization Devices

The thermoplastic mask was positioned in the path of the photon beam on the GafChromic film placed on top of the solid water phantom. The procedure was repeated as in the setup with and without the immobilizing device for the different depths and field sizes for the open beam. The set of films A, B, and C were also kept in an envelope labeled with the field size, and the presence of the thermoplastic mask (whether stretched or unstretched). The irradiated films with one unexposed film serving as control were stored for 24 hours for post-radiation exposure development. Lastly, these films were stored at a temperature of 22 ^{0}C ± 2 ^{0}C to enable stable temperature range during irradiation, storage, and scanning.

3.2.2.4 Scanning of The Irradiated Films

The exposed films were stored in envelopes for at least 24 hours at a particular temperature range to safeguard the darkening effect stabilization. Before the scanning process, the large scanner glass of the flatbed was carefully cleaned with a lint-free cloth moistened with isopropyl alcohol and a minimum of three empty scans were made to warm up the lamp of the scanner. This is to take into account the drift of the EPSON scanner on short-term (Menegotti, Delana, & Martignano, 2008). The films were removed and placed in the scanner as shown in fig 3.17 and the images were acquired in the landscape mode, as suggested by the manufacturer, because (Borca et al., 2013) explained that the lateral response artifact on EPSON STYLUS CX5900 scanners is smaller in this orientation as compared to the portrait orientation, utilizing its associated

software package "EPSON scan," used in professional mode with the image adjustments and color correction turned off, with a spatial resolution of 72 dpi in the 48 bit RGB mode (that is, 16 bit per channel) (Menegotti et al., 2008). The acquired data were saved in uncompressed tagged image file format (TIFF).

Figure 3. 17: Film placement on the scanner

3.2.2.5 Reading of The Irradiated Films (Using ImageJ)

The raw images of the irradiated films were imported into ImageJ analysis software for additional image processing. Film responses were then converted into doses (irradiated and unirradiated) and recorded in an excel worksheet. Figure 3.18 shows the ImageJ software interface with a scanned film image split into the RGB channels during the image processing and analysis.

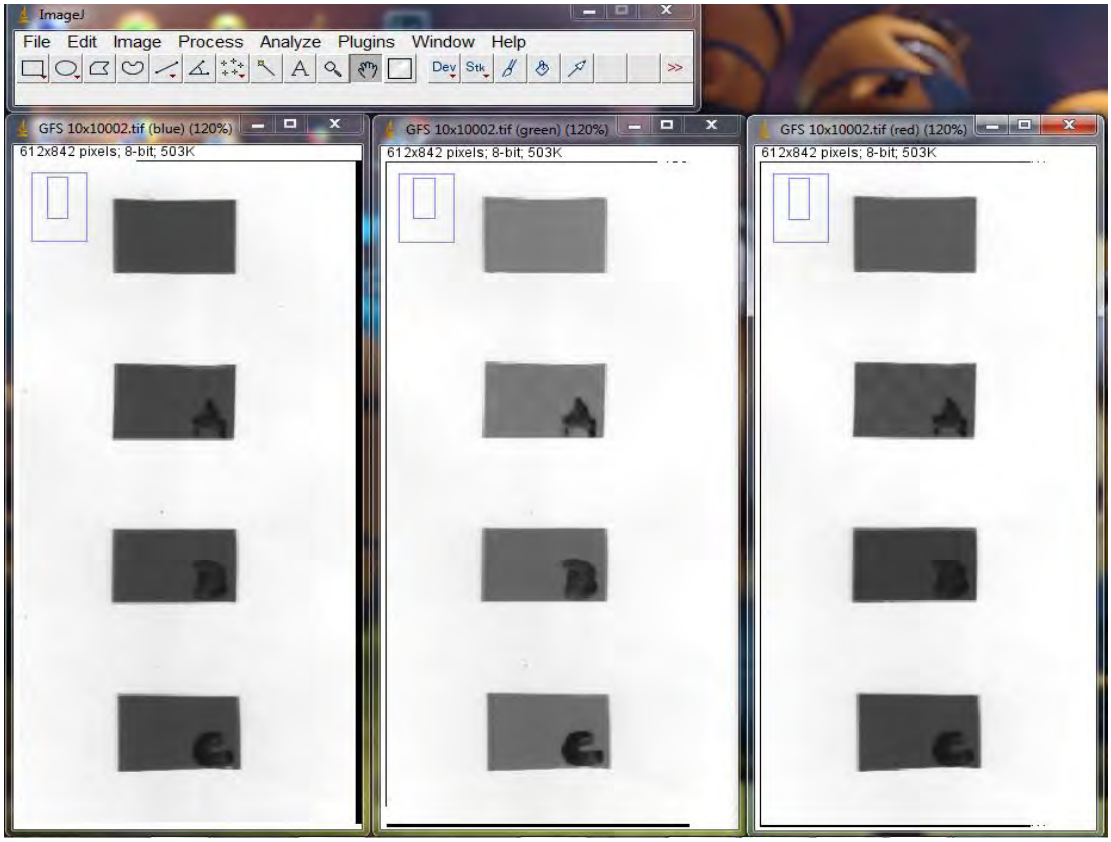

Figure 3. 18: ImageJ software interface with a scanned film image split into the RGB channels

The net optical densities of the data obtained from the mean RGB values were calculated using the following equation:

$$Net\ OD = \log_{10}\left(\frac{Unexposed\ film}{Exposed\ film}\right) \ldots\ldots\ldots (3.4)$$

3.2.3 Part 3:

3.2.3.4 Dose Verification Using the Anthropomorphic Phantom

Here the anthropomorphic phantom and the diode were used for the dose verification of the treatment plan. The phantom was first scanned using the Siemens SOMATOM Emotion 16 CT-scanner at the head and neck region in the head first supine (HFS) position. The acquired CT images were then imported into the TPS and a plan for the

target region was planned to use the 6 MV photon energy. A prescribed dose of 2 Gy was planned at the isocenter to the skin surface and the d_{max} at an SSD of 90 cm using 10 x 10 and 20 x 20 cm^2 field sizes. In the treatment room, the phantom was then irradiated as planned and the diode measured and displayed the output on the diode monitor as shown in figure 3.19. A comparison of the measured dose values and the planned dose values were done to assess the difference between the planned and delivered dose.

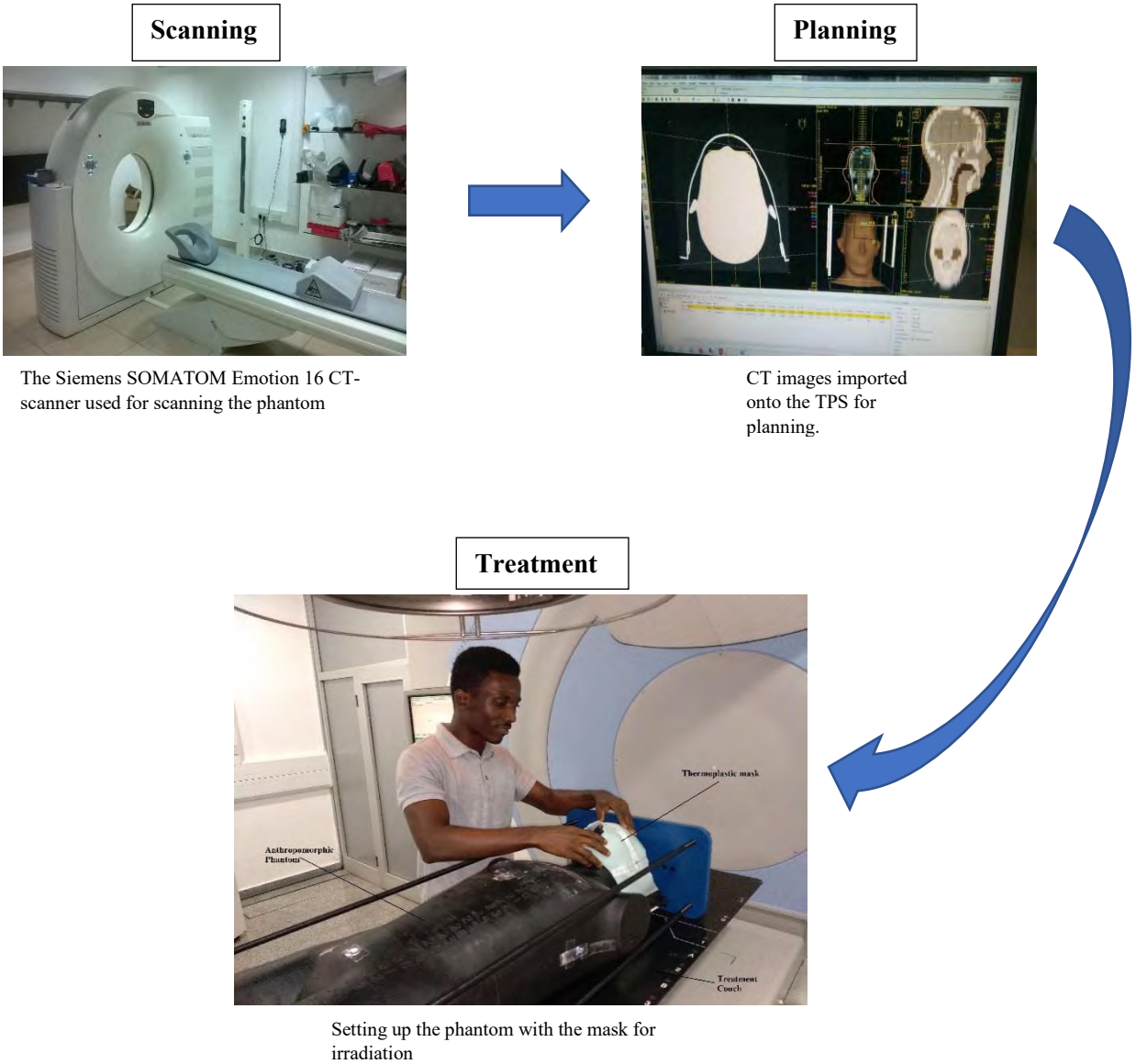

The Siemens SOMATOM Emotion 16 CT-scanner used for scanning the phantom

CT images imported onto the TPS for planning.

Setting up the phantom with the mask for irradiation

Figure 3. 19: Treatment planning process for the dose verification

CHAPTER FOUR

RESULTS AND DISCUSSION

4.1 Introduction

The use of the thermoplastics masks for immobilization during treatment of patients can be analyzed on the basis of percentage depth dose (PDD) effect, and surface dose effect on the patient. These skin dose measurements were made using the Roos type ionization chamber coupled with the UNIDOS electrometer and GafChromic EBT3 films to compare them with the values obtained from the ionization chamber. This chapter moves on to the presentation of the findings produced by the original quantitative analysis conducted as a part of this research. The raw data from all the measurements are presented in the appendices.

4.2 Dose Determination from Ion chamber

The absorbed dose at varying depths (that is, 0, 1.6, 4, 6, 8, and 10 cm) and field sizes (that is, 5 x 5, 10 x 10, 15 x 15, and 20 x 20 cm^2) of the solid water phantom was determined and tabulated. Tables 4.1 – 4.4 present the measured absorbed dose values using the Roos type ionization chamber coupled with the UNIDOS electrometer for different field sizes at different depths.

Table 4. 1: Measured Absorbed dose (Gy) values for various field sizes at different depths **without the mask**.

Depth (cm)	Field Size (cm^2) (Gy)			
	5x5	**10x10**	**15x15**	**20x20**
0	0.39	0.45	0.51	0.57
1.6	0.97	1.02	1.05	1.07
4	0.90	0.96	1.00	1.02
6	0.84	0.91	0.94	0.97
8	0.77	0.85	0.89	0.92
10	0.71	0.79	0.83	0.87

It can be observed from Table 4.1 that in the absence of the thermoplastic mask for a field size of 5 x 5 cm^2, the skin dose elevated from 0.39 to 0.97 Gy at d_{max} (1.6 cm) and later dropped to 0.71 Gy at the depth of 10 cm. Taking into consideration the skin dose, dose at maximum depth, and dose at a reference depth of 10 cm, it can be seen that with increasing field size from 5 x 5 to 20 x 20 cm^2, the skin dose increased from 0.39 to 0.57 Gy; d_{max} also increased from 0.97 to 1.07 Gy; and at the depth of 10 cm the dose increased from 0.71 to 0.87 Gy respectively. For the various field sizes, the skin dose increased by a factor of 0.06%. These results conform with literature (Hadley, Kelly, & Lam, 2005; F. M. Khan, 2014; Kry et al., 2012) since the dose gradually rises to a maximum depth where the majority of the radiation dose is deposited and falls with increasing depth within the phantom.

Table 4. 2: Measured Absorbed dose (Gy) values for various field sizes at different depths with the **unstretched mask**.

Depth (cm)	Field Size (cm^2) (Gy)			
	5x5	**10x10**	**15x15**	**20x20**
0	0.60	0.66	0.72	0.77
1.6	0.97	1.02	1.05	1.07
4	0.90	0.96	0.99	1.02
6	0.83	0.90	0.94	0.97
8	0.76	0.84	0.88	0.92
10	0.70	0.78	0.83	0.86

It can be observed from Table 4.2 that with the presence of the unstretched thermoplastic mask for a field size of 5 x 5 cm^2, the skin dose increased from 0.39 Gy (without mask) to 0.60 Gy by a factor of 0.2%. This rise in skin dose was ascribed to the "bolus" effect of the mask which shifted the d_{max} closer to the skin surface. Nevertheless, the dose at maximum depth and at the reference depth of 10 cm did not change significantly. Taking into consideration the skin dose, dose at maximum depth, and dose at a depth of 10 cm, it can be stated that with increasing field size from 5 x 5 to 20 x 20 cm^2, the skin dose increased from 0.60 to 0.77 Gy; d_{max} also increased from 0.97 to 1.07 Gy; and at the depth of 10 cm the dose increased from 0.70 to 0.86 Gy respectively. For the various field sizes, the skin dose increased by a factor of 0.06%. These results as well conform with literature (Hadley et al., 2005; F. M. Khan, 2014; Kry et al., 2012) since the dose gradually rises to a maximum depth where the majority of the radiation dose is deposited and falls with increasing depth within the phantom.

Table 4. 3: Measured Absorbed dose (Gy) values for various field sizes at different depths with the **5 cm stretched mask.**

Depth (cm)	**Field Size (cm^2) (Gy)**			
	5x5	**10x10**	**15x15**	**20x20**
0	0.52	0.58	0.64	0.70
1.6	0.99	1.04	1.07	1.09
4	0.93	0.99	1.02	1.04
6	0.86	0.93	0.97	0.99
8	0.79	0.87	0.91	0.94
10	0.73	0.81	0.86	0.89

It can as well be observed from Table 4.3 that with the presence of the 5 cm stretched thermoplastic mask for a field size of 5 x 5 cm^2, the skin dose decreased from 0.60 Gy (with the unstretched mask) to 0.52 Gy by a factor of 0.08%. This decrease in skin dose

was ascribed to the reduction in the thickness of the thermoplastic mask as a result of the stretching. However, comparing the dose at maximum depth and at the reference depth of 10 cm of the unstretched mask with the 5 cm stretched mask, it can be said that the doses changed significantly by factors of 0.02% and 0.03% respectively. Taking into consideration the skin dose, dose at maximum depth, and dose at a reference depth of 10 cm, it was observed that with increasing field size from 5 x 5 to 20 x 20 cm^2, the skin dose increased from 0.52 to 0.70 Gy; d_{max} also increased from 0.99 to 1.09 Gy; and at the depth of 10 cm the dose increased from 0.73 to 0.89 Gy respectively. These results as well conform with literature (Hadley et al., 2005; F. M. Khan, 2014; Kry et al., 2012) since the dose gradually rises to a maximum depth where the majority of the radiation dose is deposited and falls with increasing depth within the phantom.

Table 4. 4: Measured Absorbed dose (Gy) values for various field sizes at different depths with the **10 cm stretched mask**

Depth (cm)	Field Size (cm^2) (Gy)			
	5x5	**10x10**	**15x15**	**20x20**
0	0.44	0.51	0.57	0.63
1.6	0.99	1.04	1.07	1.10
4	0.93	0.99	1.02	1.04
6	0.86	0.93	0.97	1.00
8	0.80	0.87	0.91	0.94
10	0.73	0.81	0.86	0.89

It can as well be observed from Table 4.4 that with the presence of the 10 cm stretched thermoplastic mask for a field size of 5 x 5 cm^2, the skin dose decreased from 0.52 Gy (with the 5 cm stretched mask) to 0.44 Gy by a factor of 0.07%. This decrease in skin dose was as well ascribed to the further reduction in the thickness of the thermoplastic mask as a result of the stretching. However, comparing the dose at maximum depth and

at a depth of 10 cm of the 5 cm stretched mask with the 10 cm stretched mask, it can be said that the doses did not change significantly. Taking into consideration the skin dose, dose at maximum depth, and dose at a reference depth of 10 cm, it was observed that with increasing field size from 5 x 5 to 20 x 20 cm^2, the skin dose increased from 0.44 to 0.63 Gy; d_{max} also increased from 0.99 to 1.09 Gy; and at the depth of 10 cm the dose increased from 0.73 to 0.89 Gy respectively. These results also conform with literature (Hadley et al., 2005; F. M. Khan, 2014; Kry et al., 2012) since the dose gradually rises to a maximum depth where the majority of the radiation dose is deposited and falls with increasing depth within the phantom.

4.2.1 Graphical Representations of Absorbed Dose against Depth

The figures 4.1 – 4.4 are the graphical representations of the absorbed doses obtained using the ionization chamber against depth as tabulated in Table 4.1 – 4.4 respectively.

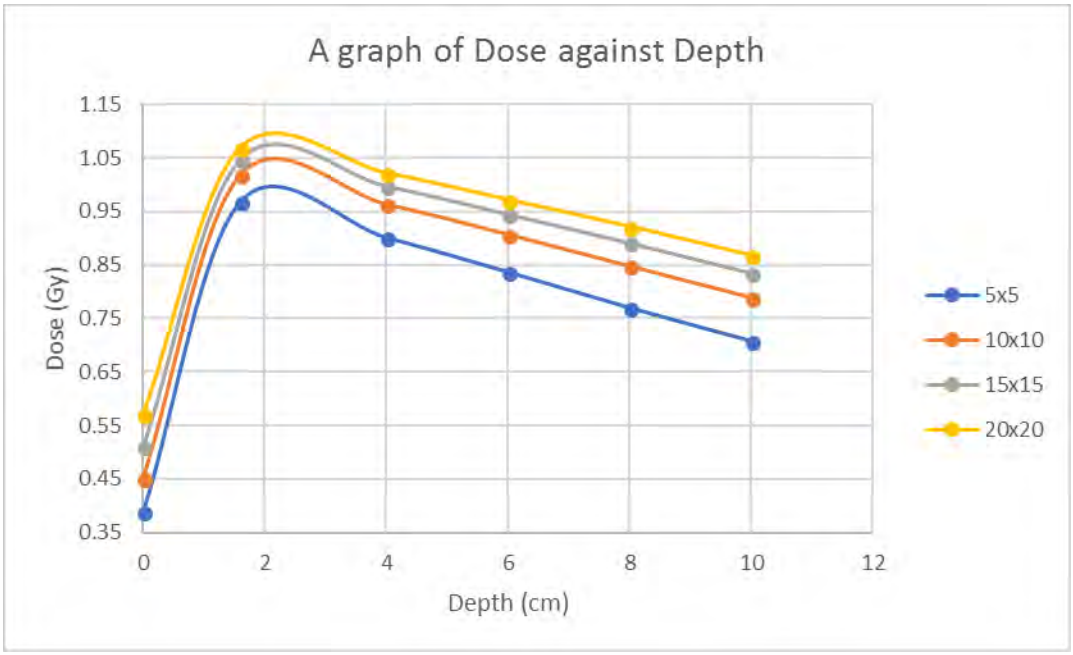

Figure 4. 1: A graphical representation of Absorbed dose against Depth for **no thermoplastic mask.**

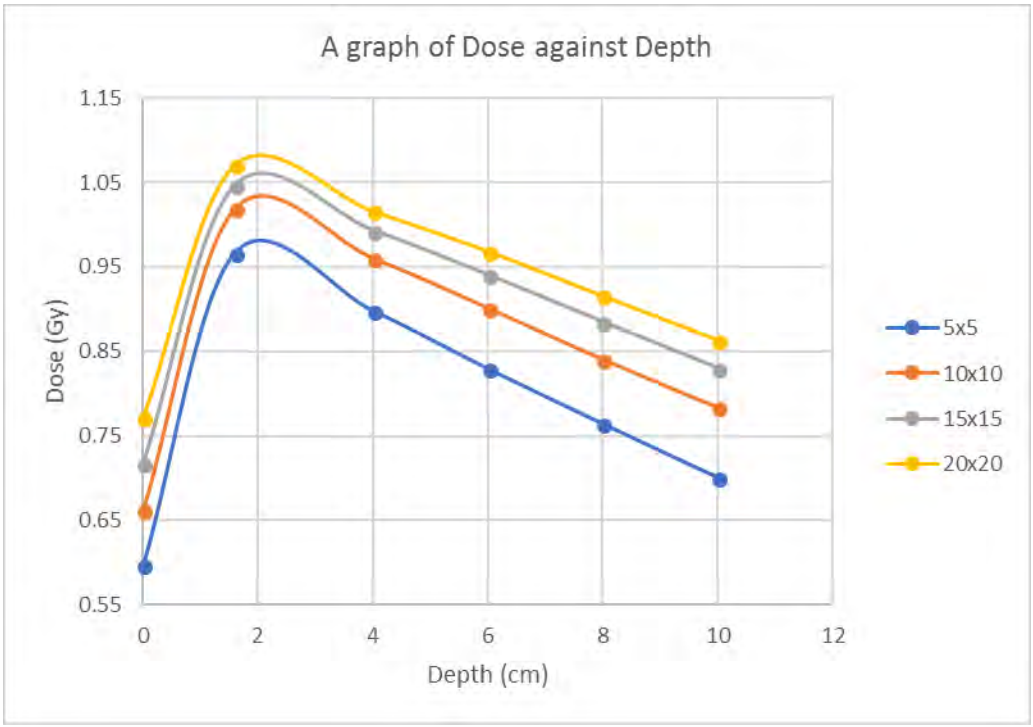

Figure 4. 2: A graphical representation of Absorbed dose against Depth for the **unstretched thermoplastic mask**.

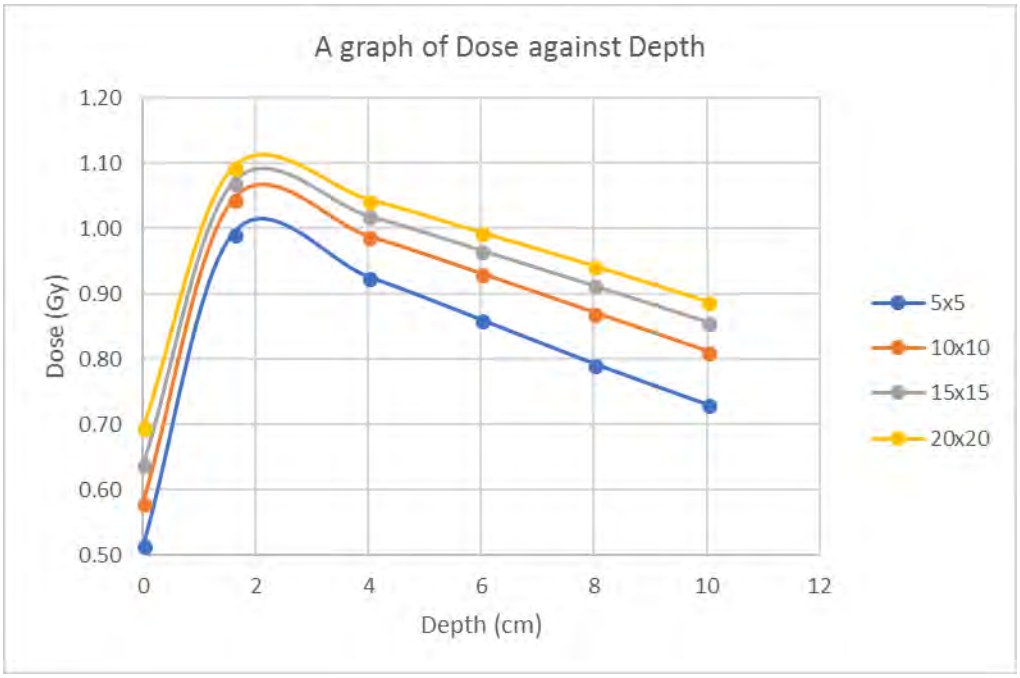

Figure 4. 3: A graphical representation of Absorbed dose against Depth for the **5 cm stretched thermoplastic mask**.

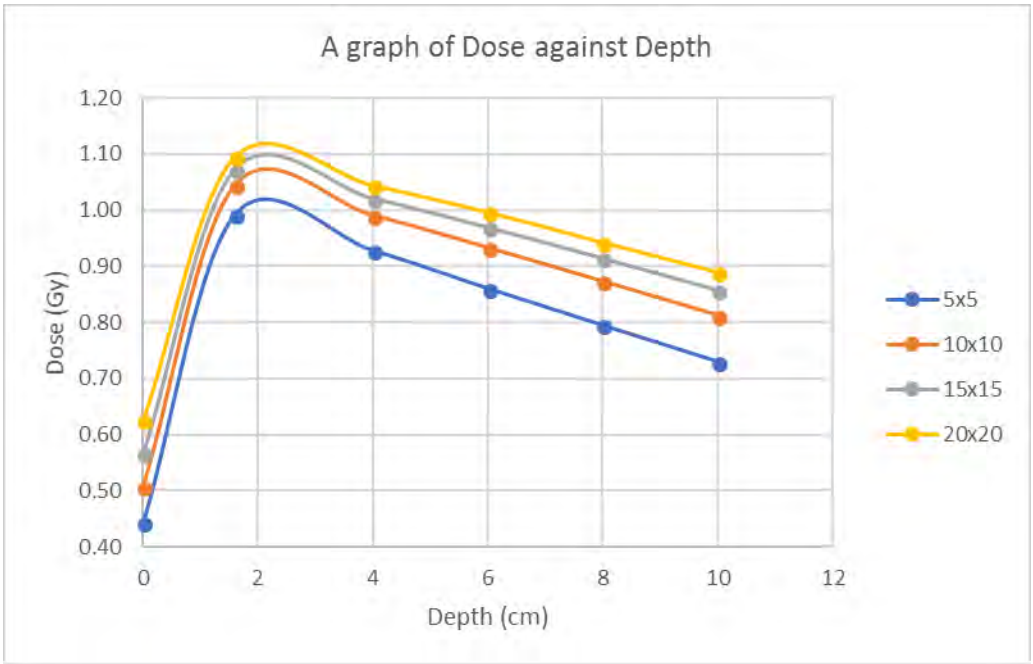

Figure 4. 4: A graphical representation of Absorbed dose against Depth for the **10 cm stretched thermoplastic mask**.

4.3 Percentage Depth Dose (PDD) Determination

The determination of the percentage depth dose with and without the thermoplastic mask made it easy to assess the build-up effect of the thermoplastic mask on the skin. Figures 4.5 – 4.7 show a graph of percentage depth dose against depth with or without the mask for a 10 x 10 cm^2 field size.

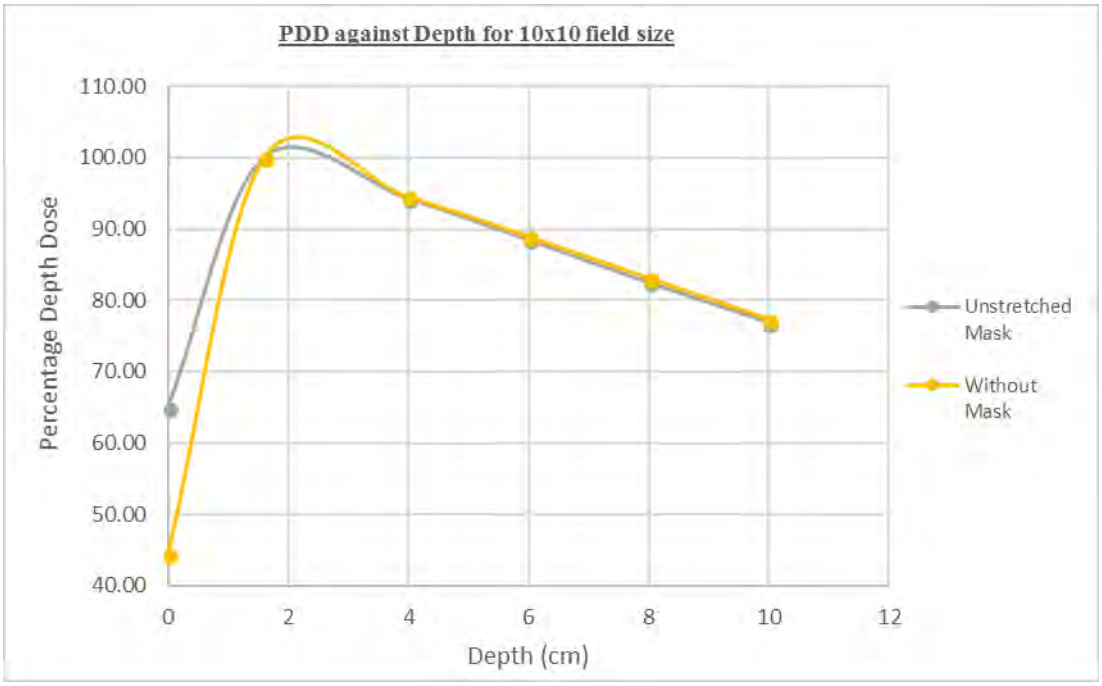

Figure 4. 5: A graph of PDD against Depth for a 10x10 field size with an unstretched mask and without a mask.

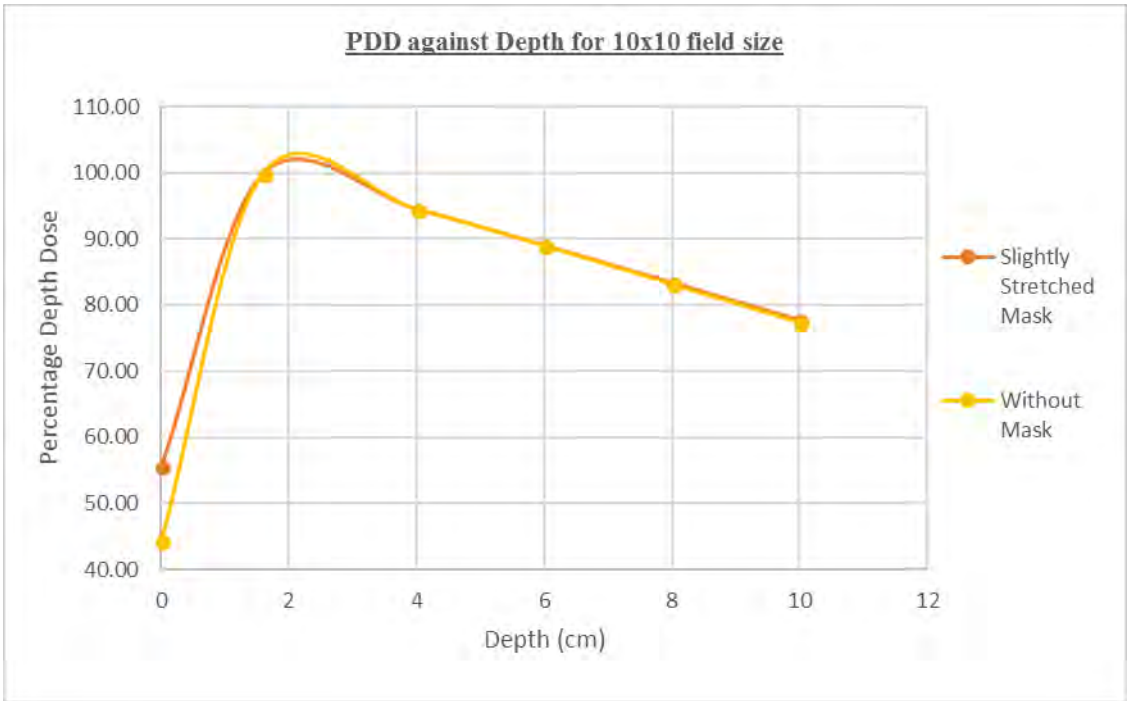

Figure 4. 6: A graph of PDD against Depth for a 10x10 field size with a 5 cm stretched mask and without a mask.

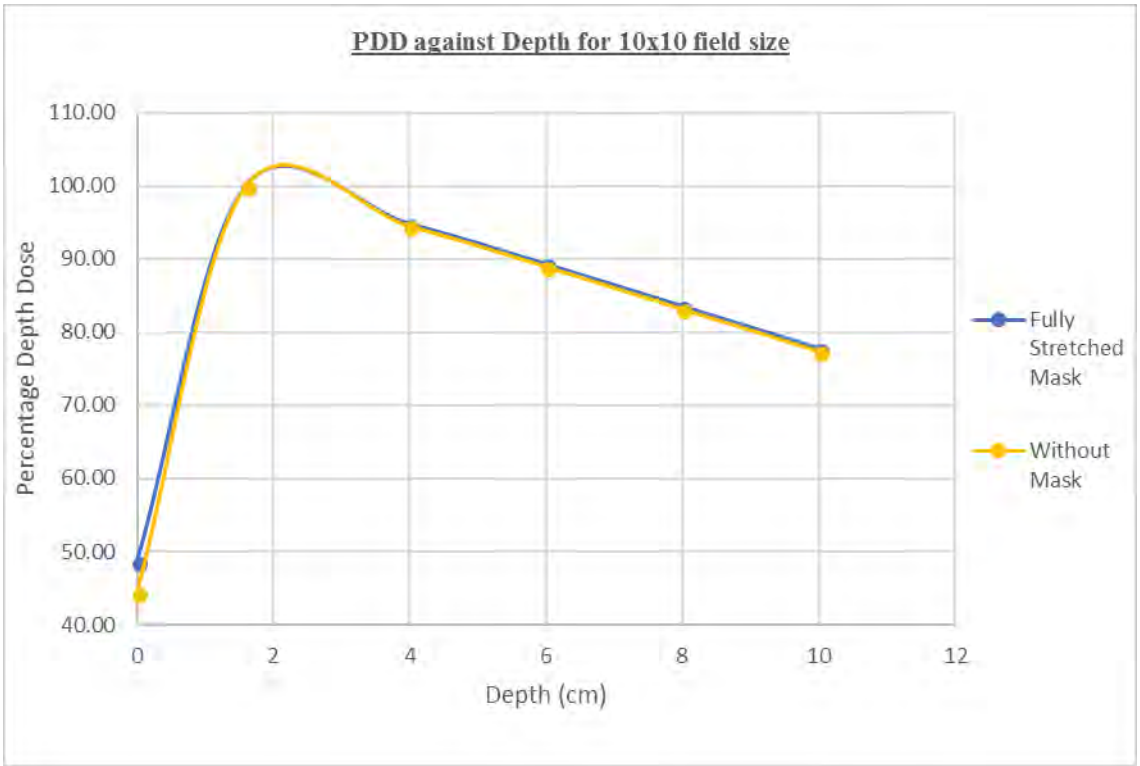

Figure 4. 7: A graph of PDD against Depth for a 10 x 10 field size with a 10 cm stretched mask and without a mask.

Due to the presence of the thermoplastic mask during measurements, the depth dose in the build-up region increased, subsequently shifting of the d_{max} to increasingly lower depths to the skin surface. For a field size of 10 x 10 cm, an increase in skin dose of **0.21, 0.13 and 0.05 Gy** were estimated for the unstretched mask, the 5 cm stretched mask and the 10 cm stretched mask respectively, which was ascribed to the "bolus" effect of the thermoplastic masks.

4.3.1 Variation of Percentage Depth Dose (PDD) with Field Size and Depth.

Field size, which is a scatter factor is proportional to percentage depth dose. The influence of the scattered radiation to the absorbed dose at a point in the patient or phantom increases with respect to field size and therefore the increase in scattered dose

occurs at greater depths than at the depth of maximum dose (d_{max}) causing an increase in dose. The PDD increased from the surface to a d_{max} (1.6 cm) and then decreased with increasing depth. The variation in percentage depth dose as a function of the field size and depth for the various thicknesses of the thermoplastic mask are represented in figures 4.8 - 4.11.

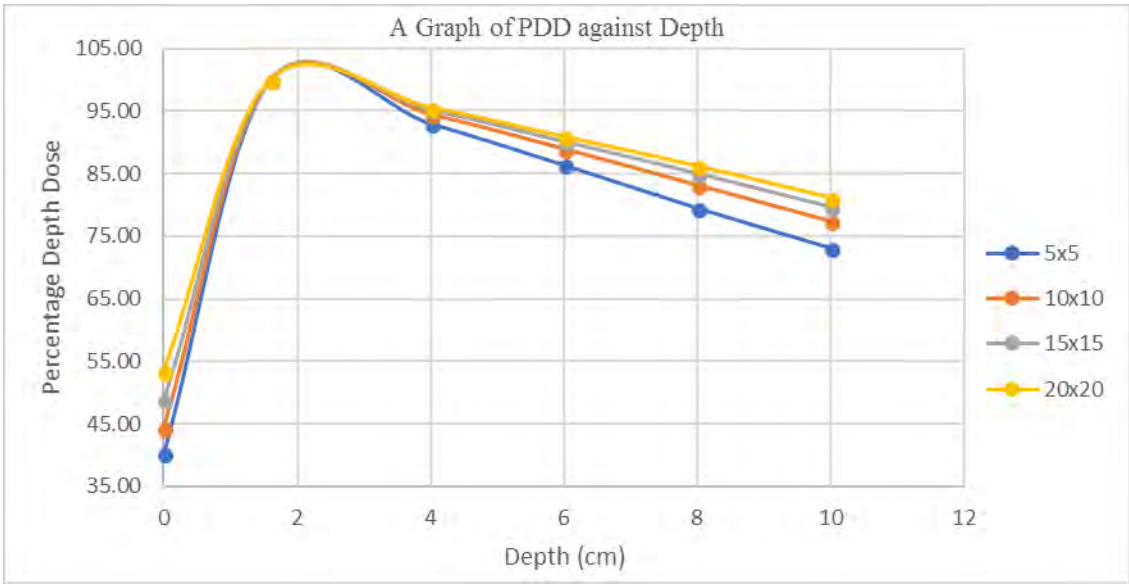

Figure 4. 8: A graph showing the variation of PDD versus depth and field size for measurements **without the thermoplastic mask.**

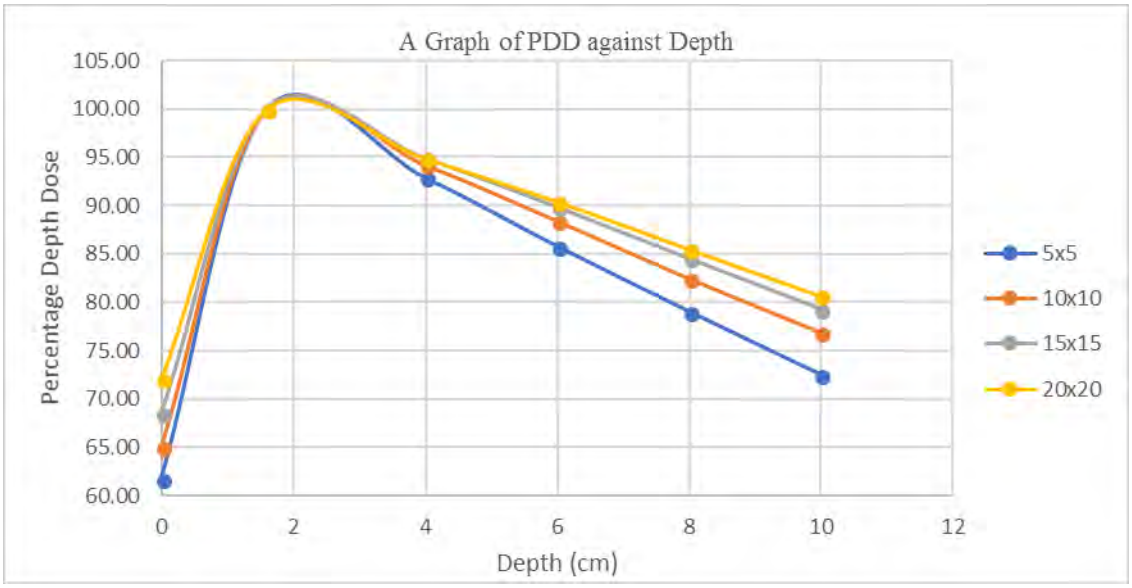

Figure 4. 9: A graph showing the variation of PDD versus depth and field size for measurements with an **unstretched thermoplastic mask.**

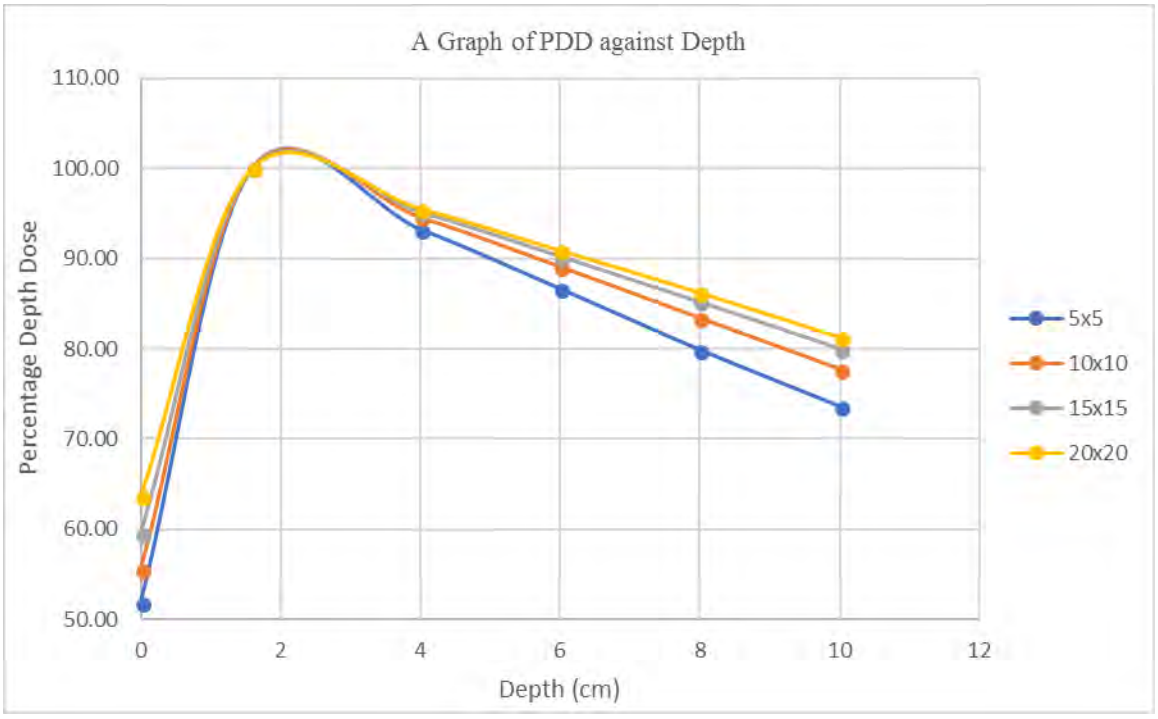

Figure 4. 10: A graph showing the variation of PDD versus depth and field size for measurements with a **5 cm stretched thermoplastic mask.**

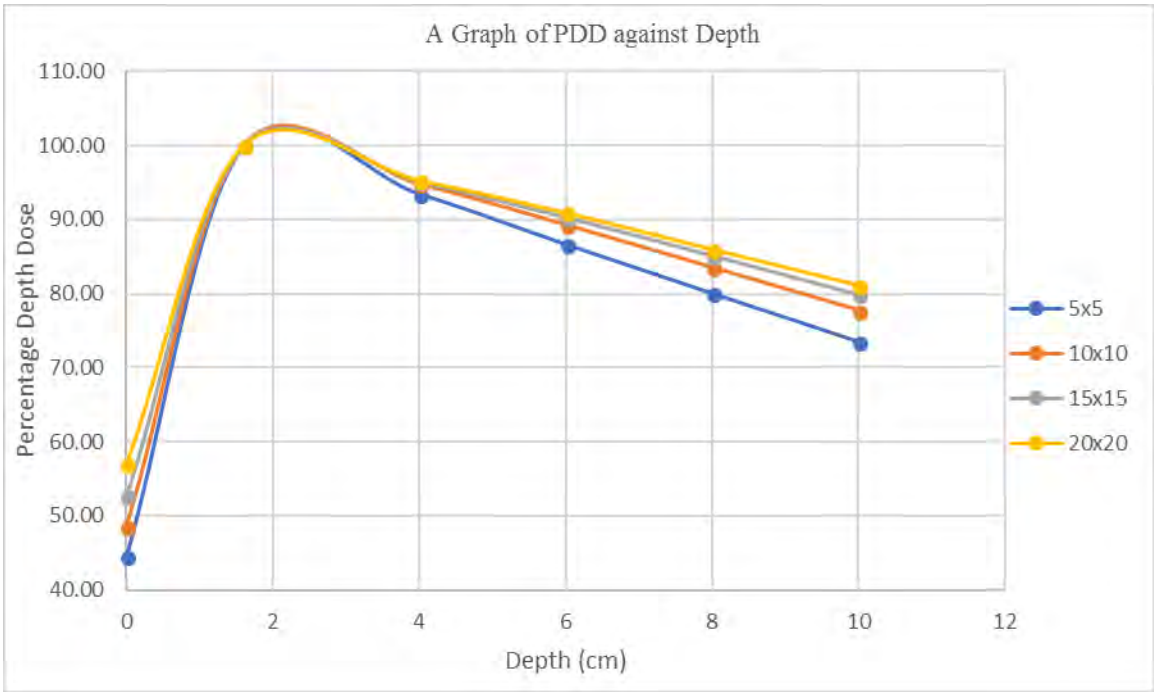

Figure 4. 11: A graph showing the variation of PDD versus depth and field size for measurements with a **10 cm stretched thermoplastic mask.**

4.4 Determination of Skin Dose from PDD values

From figure 4.12, the percentage depth dose measurements without the thermoplastic mask at 0.0 cm depth was compared to the percentage depth dose measurements at a depth of 0.0 cm with the various thermoplastic masks (that is, unstretched, 5 cm and 10 cm stretched masks). It can be seen that the presence of the thermoplastic mask as an immobilizing device shifted the d_{max} closer to the skin thereby causing an increase in the skin dose. Taking into consideration the field size of 10 x 10 cm^2, a PDD of 44.42 was recorded for the measurements without the mask and increased to 48.61, 55.61, and 64.98 for the measurements with the 10 cm stretched mask, 5 cm stretched mask and the unstretched mask respectively at a depth of 0.0 cm. As the field sizes increased for a particular thermoplastic mask thickness, the skin dose also increased, with the

unstretched mask recording the highest followed by the 5 cm stretched mask; 10 cm stretched mask, and no mask recording the least skin dose.

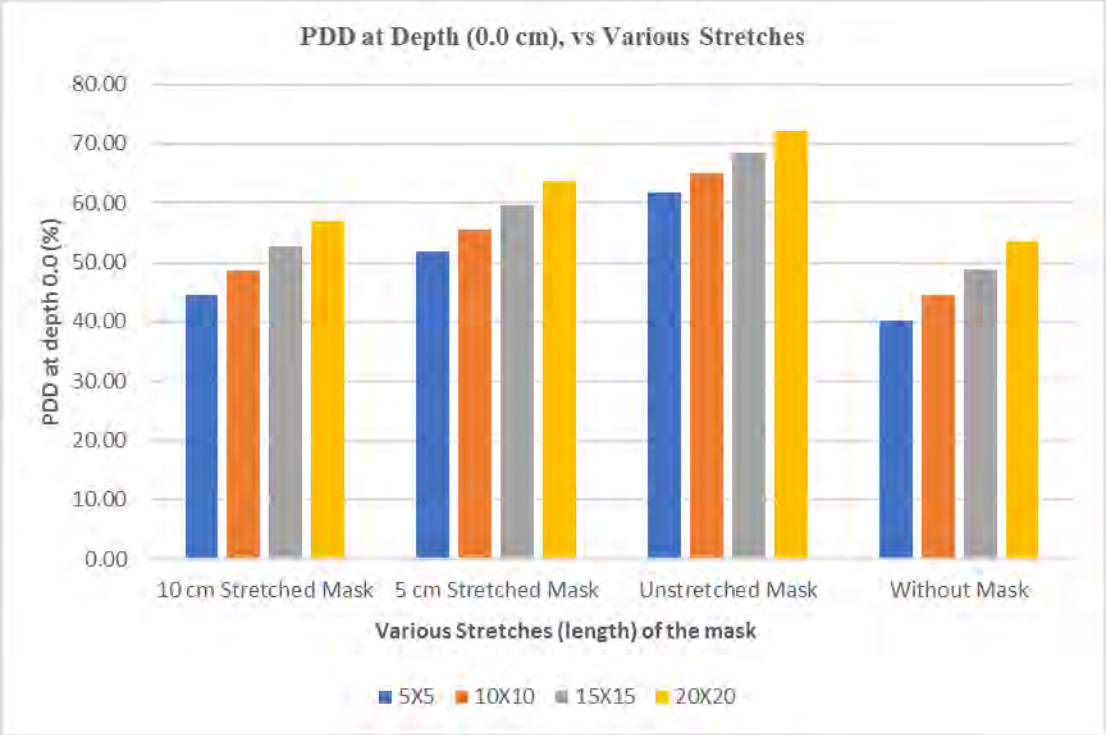

Figure 4. 12: A bar chart showing the effect of different mask thickness on PDD at depth 0.0 cm.

Figure 4.13 also illustrates a plot of skin dose at different field sizes against the various mask stretches. The difference in skin doses for the various stretches was compared with the measurement without the mask at the different field sizes and tabulated below in Table 4.5. A variation within 1% was recorded although the skin dose decreased as the mask was extended.

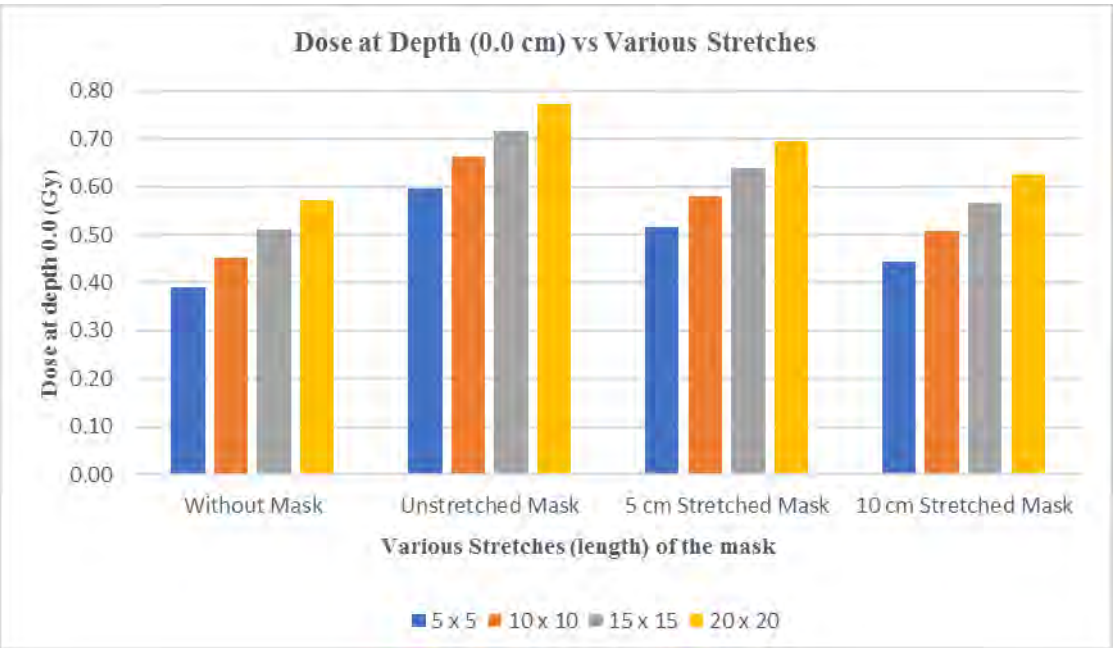

Figure 4. 13: A bar chart showing the effect of different mask thickness on the skin dose at depth 0.0 cm.

Table 4. 5: Dose (Gy) differences between the various mask stretches and without the mask

Field sizes (cm^2)	Without Mask	Unstretched Mask	5 cm Stretched Mask	10 cm Stretched Mask
5 x 5	0.39	0.21	0.13	0.05
10 x 10	0.45	0.21	0.13	0.05
15 x 15	0.51	0.21	0.13	0.05
20 x 20	0.57	0.20	0.12	0.05

The skin-sparing effect which is a significant factor of higher energy beams was achieved when there was no mask present and also when the 10 cm stretched mask was used. On the other hand, when the thermoplastic mask was overstretched to minimize the build-up effect and increase the skin sparing effect, the masks rigidity was compromised thus reducing its ability to function properly as an immobilization device. Figure 4.13 above illustrates the increase in skin dose due to the presence of the thermoplastic mask at various field sizes.

4.4.1 Effect of Field Size on Skin Dose.

As mentioned in literature, field size is one of the factors that affect a patient's skin dose. Table 4.6 shows an increase in skin doses as the field size was increased for different thermoplastic mask stretches. The increase in skin dose with increasing field size was manifested in both measurements with and without the thermoplastic mask. The increasing skin dose was associated with the increase in electron scattering from the air, the collimators any other materials in the path of the radiation beam. A skin dose of 0.60 Gy was measured at a field size of 5 x 5 cm^2 and later increased to 0.77 Gy at a field size of 20 x 20 cm^2 for the unstretched mask. This conforms with other results in literature (Hadley et al. 2005; Khan, 2014; Kry, Smith et al. 2012), which stated an increase in skin dose with increasing field size.

Table 4. 6: Skin Doses (Gy) at a depth of 0.0 cm for the various Stretches of the thermoplastic mask.

Field sizes (cm^2)	Without Mask	10 cm Stretched Mask	5 cm Stretched Mask	Unstretched Mask
5X5	0.39	0.44	0.52	0.60
10X10	0.45	0.51	0.58	0.66
15X15	0.51	0.57	0.64	0.72
20X20	0.57	0.63	0.70	0.77

4.4.2 Verification of Prescribed Dose

The data obtained after the dose verification was compared to the delivered dose at both the skin surface and the d_{max}. With or without the mask, the surface dose increased with increasing field size. The skin dose increased whilst the d_{max} shifted closer to the skin surface due to the "bolus" effect of the mask present. The percentage differences obtained

were all less than 1% which falls within the tolerance limit of ±1%. The acquired data are presented in appendix 11.

4.5 Thermoplastic Factors, TF

The thermoplastic mask factor as stated in chapter three is expressed as a ratio of the corrected ion chamber readings with mask I_1 to that without mask I_0. The values in the Tables 4.7, 4.8 and 4.9 were obtained using equation **(3.3)**. Tables 4.7 – 4.9 present the thermoplastic factors obtained from the stretched and unstretched thermoplastic masks at varying depths and field sizes. A close observation of Tables 4.7 – 4.9 clearly show that the unstretched mask had higher thermoplastic factors at the skin surface (that is, at depth 0.0 cm) followed by the 5 cm stretched mask with the 10 cm stretched masks having the lowest for all the different field sizes. The thicker the mask, the higher the thermoplastic factor at the skin surface. As the depth increased beyond the skin surface within the phantom, the thermoplastic factor of the 10 cm stretched mask increased significantly followed by the 5 cm stretched mask with the unstretched mask having the least values. For a particular mask type (unstretched, 5 cm stretched, or 10 cm stretched) the thermoplastic factor decreased with increasing field size.

Table 4. 7: Thermoplastic factor for the **unstretched thermoplastic mask**.

Depth (cm)	Field Size (cm^2)			
	5x5	10x10	15x15	20x20
0	1.535902	1.4631	1.40447	1.35071
1.6	0.999406	1.00028	1.00027	1.00242
4	0.997445	0.99701	0.99654	0.99549
6	0.992125	0.99398	0.99634	0.99763
8	0.993163	0.99169	0.99354	0.99438
10	0.990775	0.99337	0.99493	0.99635

Table 4. 8: Thermoplastic factor for the **5 cm stretched thermoplastic mask.**

Depth (cm)	Field Size (cm^2)			
	5x5	10x10	15x15	20x20
0	1.322636	1.28119	1.24728	1.215943
1.6	1.024368	1.02342	1.02225	1.021798
4	1.026509	1.02388	1.02164	1.021408
6	1.02703	1.02473	1.02284	1.021913
8	1.028693	1.02653	1.02357	1.022167
10	1.031169	1.02832	1.02619	1.023549

Table 4. 9: Thermoplastic factor for the **10 cm stretched thermoplastic mask.**

Depth (cm)	Field Size (cm^2)			
	5x5	10x10	15x15	20x20
0	1.138357	1.121634	1.107547	1.094308
1.6	1.025557	1.025113	1.025	1.025565
4	1.030661	1.027463	1.023947	1.023099
6	1.029334	1.028218	1.0265	1.026355
8	1.03299	1.029242	1.026154	1.023416
10	1.032063	1.029488	1.02733	1.026202

4.6 Calibration Curve

Table 4.10 gives the measured net optical density (Net OD) as a function of absorbed dose (Gy) for the calibrated GafChromic EBT3 films. These optical densities were obtained from equation (3.4) in chapter three. Figure 4.14 also illustrates a plot of calculated net optical densities against the known absorbed doses for the calibrated GafChromic EBT3 film.

Table 4. 10: Net Optical Densities as a function of absorbed dose for the calibrated GafChromic films

Absorbed Dose (Gy)	Red	Green	Blue
0	0	0	0
0.20	0.04376	0.016714	0.00103
0.40	0.07846	0.032179	0.00465
0.80	0.13711	0.066814	0.01564
1.60	0.22021	0.127031	0.03478
2.40	0.2696	0.177514	0.05165
3.20	0.3015	0.220504	0.06437
4.00	0.32749	0.254787	0.07766
5.00	0.35221	0.301327	0.09495

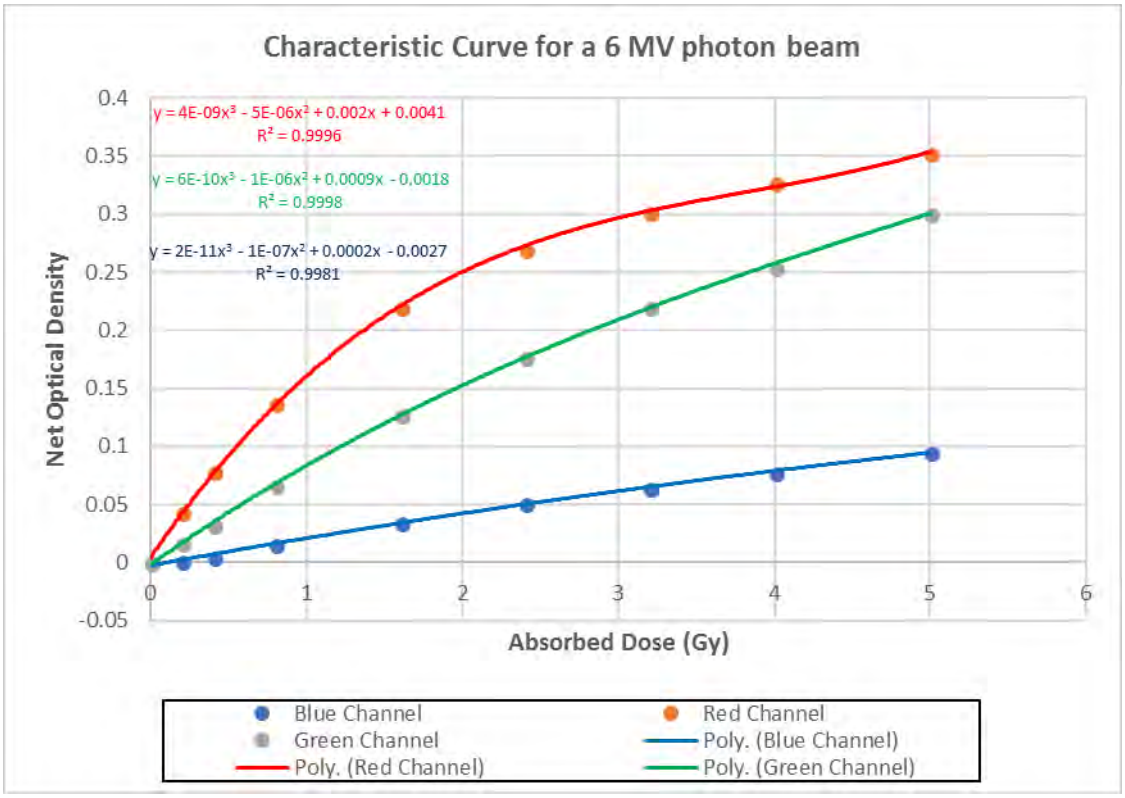

Figure 4. 14: Calibration curve comparing RGB channels for 6 MV photon energy.

A close observation of figure 4.14 illustrates the calibration curve for the RGB channels using a 6 MV energy where the red channel is said to give a better dose variation and higher sensitivity as compared to the green and blue channels. From (Borca et al., 2013b),

the red channel had a larger response up to 10 Gy with the green channel exceeding the red one for radiation doses above 10 Gy. On the other hand, the blue channel had a lower response gradient at any dose because the signal has a weak dose dependence while having a strong dependence on the thickness of the active layer. Thus, this makes the blue channel less suitable than the other channels for dose measurements. Consequently, further analysis was done on the red channels. Figure 4.15 shows a plot of absorbed dose against net optical density for the selected red channel.

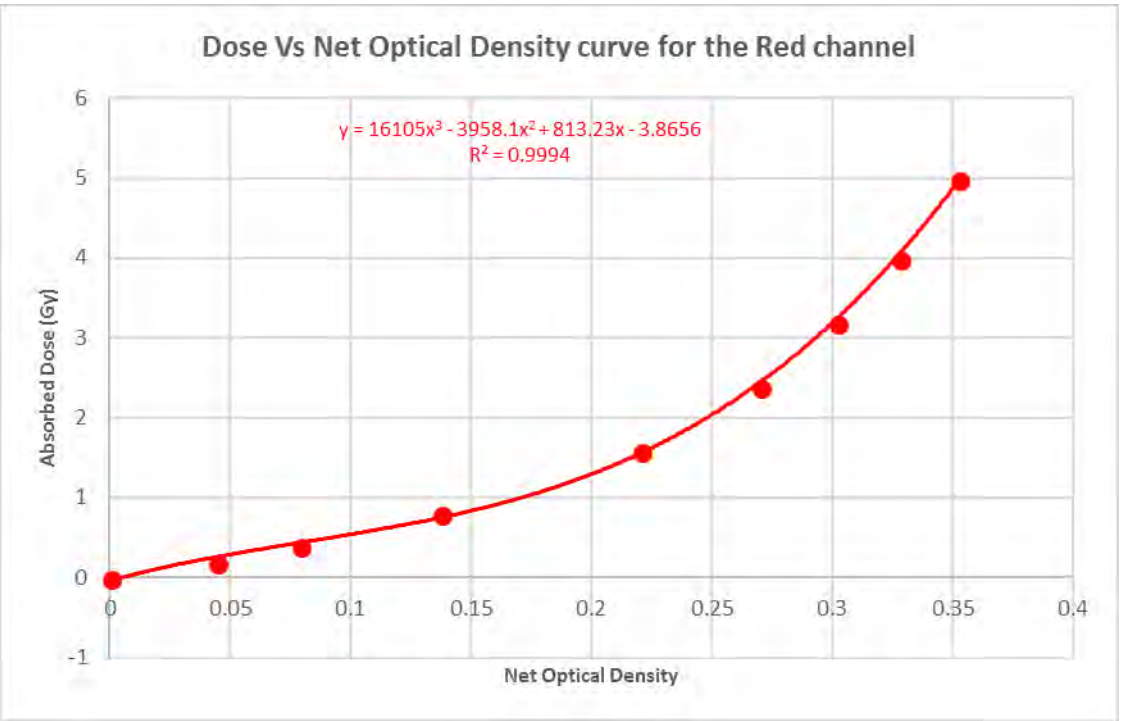

Figure 4. 15: A graph of Absorbed Dose against Net Optical Density for the Red channel.

The corresponding calibration equation obtained from figure 4.15 for the conversion of the other film responses to dose is given by equation **(4)**

$$y = a + bx + cx^2 + dx^3 + ex^4 + \ldots \quad \ldots\ldots\ldots (4)$$

where **a = -3.8656, b = 813.23, c = -3958.1, d = 16105** and the regression **R^2 = 0.9994.**

4.6.1 Dose Determination for the Irradiated GafChromic EBT3 Films.

4.6.1.1 Net Optical Density (Net OD)

Tables 4.11 – 4.14 illustrate the Net Optical Densities (Net OD) obtained after the scanning and reading of the GafChromic films which were irradiated with the unknown radiation doses.

Table 4. 11: Net Optical Densities (Net OD) obtained for the GafChromic films **without the mask.**

Depth (cm)	Field size (cm^2)			
	5 x 5	10 x 10	15 x 15	20 x 20
0.0	0.03844	0.05005	0.07276	0.07655
1.6	0.17499	0.1871	0.18661	0.18521
10.0	0.12877	0.13628	0.14948	0.14728

Table 4. 12: Net Optical Densities (Net OD) obtained for the GafChromic films with the **unstretched mask.**

Depth (cm)	Field size (cm^2)			
	5 x 5	10 x 10	15 x 15	20 x 20
0.0	0.11937	0.12846	0.131	0.14826
1.6	0.18217	0.19709	0.18861	0.1962
10.0	0.13031	0.14469	0.13631	0.14736

Table 4. 13: Net Optical Densities (Net OD) obtained for the GafChromic films with the **5 cm stretched mask.**

Depth (cm)	Field size (cm^2)			
	5 x 5	10 x 10	15 x 15	20 x 20
0.0	0.08675	0.10143	0.10836	0.10821
1.6	0.17619	0.18442	0.19683	0.18637
10.0	0.12888	0.13613	0.15135	0.13732

Table 4. 14: Net Optical Densities (Net OD) obtained for the GafChromic films with the **10 cm stretched mask.**

Depth (cm)	Field size (cm^2)			
	5 x 5	10 x 10	15 x 15	20 x 20
0.0	0.08193	0.06123	0.09666	0.09611
1.6	0.19743	0.18116	0.19317	0.18977
10.0	0.14362	0.13692	0.15554	0.15079

4.6.1.2 GafChromic Film Doses

The above-tabulated net optical densities with and without the thermoplastic mask for the various depths and field sizes were used to determine the doses deposited in the GafChromic films. These were done by using equation **(4.1)** from the calibration curve of the absorbed dose against the net optical density:

$$y = 16105x^3 - 3958.1x^2 + 813.23x - 3.8656 \quad \ldots\ldots\ldots (4.1)$$

Tables 4.15 – 4.18 represent the calculated absorbed doses acquired from the GafChromic films using equation **(4.1)**.

Table 4. 15: Calculated absorbed dose (Gy) values for various field sizes at different depths **without the mask.**

Depth (cm)	Field size (cm^2)			
	5 x 5	10 x 10	15 x 15	20 x 20
0	0.22	0.29	0.41	0.42
1.6	1.04	1.15	1.15	1.13
10	0.70	0.74	0.83	0.82

A close observation of Table 4.15 shows that in the absence of the thermoplastic mask for the field size of 10 x 10 cm^2, the surface dose elevated from 0.29 Gy to 1.15 Gy at d_{max} (1.6 cm) and later dropped to 0.74 Gy at the reference depth of 10 cm. Taking into consideration the skin dose, dose at maximum depth, and dose at a reference depth of 10

cm, it can be seen that with increasing field size from 5 x 5 to 20 x 20 cm^2 the skin dose increased from 0.22 Gy to 0.42 Gy; d_{max} also increased from 1.04 Gy of 5 x 5 field size to 1.15Gy at a field size of 10 x 10 and later dropped to 1.13 Gy at 20 x 20 field size; and at the reference depth of 10 cm the dose increased from 0.70 Gy to 0.83Gy of field size of 15 x15 and also dropped to 0.82 Gy at a field size of 20 x 20 respectively. For the various field sizes, the skin dose increased by a factor of 0.06% (for 5 x 5 to 10 x 10 cm^2), 0.11% (for 10 x 10 to 15 x 15 cm^2), and 0.02% (for 5 x 5 to 10 x 10 cm^2). Thus, these results conform with literature on the aspect of increasing depth for a particular field size but deviate from literature in the aspect of increasing field sizes for d_{max} (1.6 cm) and a depth of 10 cm as indicated in (F. M. Khan, 2014).

Table 4. 16: Calculated absorbed dose (Gy) values for various field sizes at different depths with the **unstretched mask**.

Depth (cm)	Field size (cm^2)			
	5 x 5	10 x 10	15 x 15	20 x 20
0	0.64	0.69	0.71	0.82
1.6	1.10	1.26	1.17	1.25
10	0.71	0.80	0.74	0.82

A close observation of Table 4.16 shows that the presence of the unstretched mask for a field size of 10 x 10 cm^2, the surface dose increased from 0.29 Gy (without the mask) to 0.69 Gy by a factor of 0.38%. The rise in skin dose was ascribed to the "bolus" effect due to the presence of the mask. However, comparing the dose at maximum depth and at the reference depth of 10 cm without a mask with the unstretched mask, it can be said that there was an insignificant change in the dose values. Also, the skin dose for the unstretched mask raised from 0.69 Gy to 1.26 Gy at d_{max} (1.6 cm) and later dropped to 0.80 Gy at the depth of 10 cm. Taking into account the skin dose, dose at maximum

depth, and dose at a reference depth of 10 cm, it can be seen that with increasing field size from 5 x 5 to 20 x 20 cm^2 the skin dose increased from 0.64 Gy to 0.82 Gy; d_{max} had fluctuations within the various field sizes; and at the depth of 10 cm the dose also fluctuated within the field sizes respectively. For the various field sizes, the skin dose increased by a factor of 0.06% (for 5 x 5 to 10 x 10 cm^2), 0.11% (for 10 x 10 to 15 x 15 cm^2), and 0.02% (for 5 x 5 to 10 x 10 cm^2). Thus, these results conform with literature on the aspect of increasing depth for a particular field size but deviate from literature in the aspect of increasing field sizes for d_{max} (1.6 cm) and a depth of 10 cm as indicated in(Hadley et al., 2005; F. M. Khan, 2014; Kry et al., 2012).

Table 4. 17: Calculated absorbed dose (Gy) values for various field sizes at different depths with the **5 cm stretched mask.**

Depth (cm)	Field size (cm^2)			
	5x5	10x10	15x15	20x20
0	0.47	0.55	0.58	0.58
1.6	1.05	1.13	1.26	1.14
10	0.70	0.74	0.84	0.75

A close observation of Table 4.17 shows that with the presence of the 5 cm stretched mask for a field size of 10 x 10 cm^2, the surface dose decreased from 0.69 Gy (with the unstretched mask) to 0.55 Gy by a factor of 0.17%. The decrease in skin dose was as well attributed to the reduction in the thickness of the mask as a result of the slight stretching. However, comparing the dose at maximum depth and at the reference depth of 10 cm of the unstretched mask with the 5 cm stretched one, it can be said that there was an insignificant change in the dose values by factors of 0.05% and 0.008%. Considering the skin dose, dose at maximum depth, and dose at a reference depth of 10 cm, while increasing field size from 5 x 5 to 20 x 20 cm^2, the skin dose increased from 0.47 Gy to

0.58 Gy; d_{max} had fluctuations within the different field sizes; and at the depth of 10 cm the dose also fluctuated within the field sizes respectively. For the various field sizes, the skin dose increased by a factor of 0.07% (for 5 x 5 to 10 x 10 cm^2), 0.04% (for 10 x 10 to 15 x 15 cm^2), and 0.0008% (for 5 x 5 to 10 x 10 cm^2). Thus, these results conform with literature on the aspect of increasing depth for a particular field size but deviate from literature in the aspect of increasing field sizes for d_{max} (1.6 cm) and a depth of 10 cm as indicated in (Hadley et al., 2005; F. M. Khan, 2014; Kry et al., 2012).

Table 4. 18: Calculated absorbed dose (Gy) values for various field sizes at different depths with the **10 cm stretched mask.**

Depth (cm)	Field size (cm^2)			
	5x5	10x10	15x15	20x20
0	0.45	0.35	0.52	0.52
1.6	1.26	1.09	1.22	1.18
10	0.79	0.75	0.87	0.84

From the observation of Table 4.18, it shows that with the presence of the 10 cm stretched mask for a field size of 10 x 10 cm^2, the surface dose decreased from 0.55 Gy (with the 5 cm stretched mask) to 0.35 Gy by a factor of 0.086%. This decrease in the skin dose was as well attributed to the reduction in the thickness of the mask as a result of the full stretching. However, comparing the dose at maximum depth and at a reference depth of 10 cm of the 5 cm stretched mask with the 10 cm stretched one, it can be deduced that there was an insignificant change in the dose values by factors of 0.05% and 0.06%. Considering the skin dose, dose at maximum depth, and dose at a reference depth of 10 cm, while increasing field size from 5 x 5 to 20 x 20 cm^2, the skin dose fluctuated between 0.35 Gy and 0.52 Gy; d_{max} had fluctuations within the different field sizes; and at

the depth of 10 cm the dose also fluctuated within the field sizes respectively. Thus, these results conform with literature on the aspect of increasing depth for a particular field size but deviate from literature in the aspect of increasing field sizes for a particular depth as indicated in (Hadley et al., 2005; F. M. Khan, 2014; Kry et al., 2012).

4.6.1.2.1 Graphical Representations of Absorbed dose against Depth for the GafChromic film.

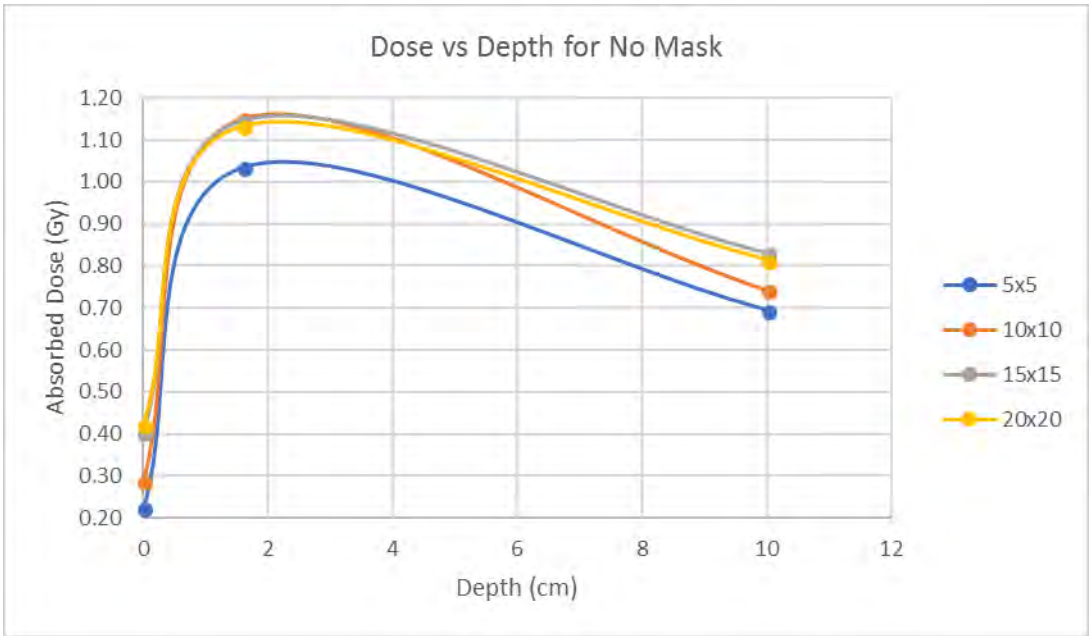

Figure 4. 16: A graph showing the variation of absorbed dose versus depth and field size for GafChromic measurements **without the mask**.

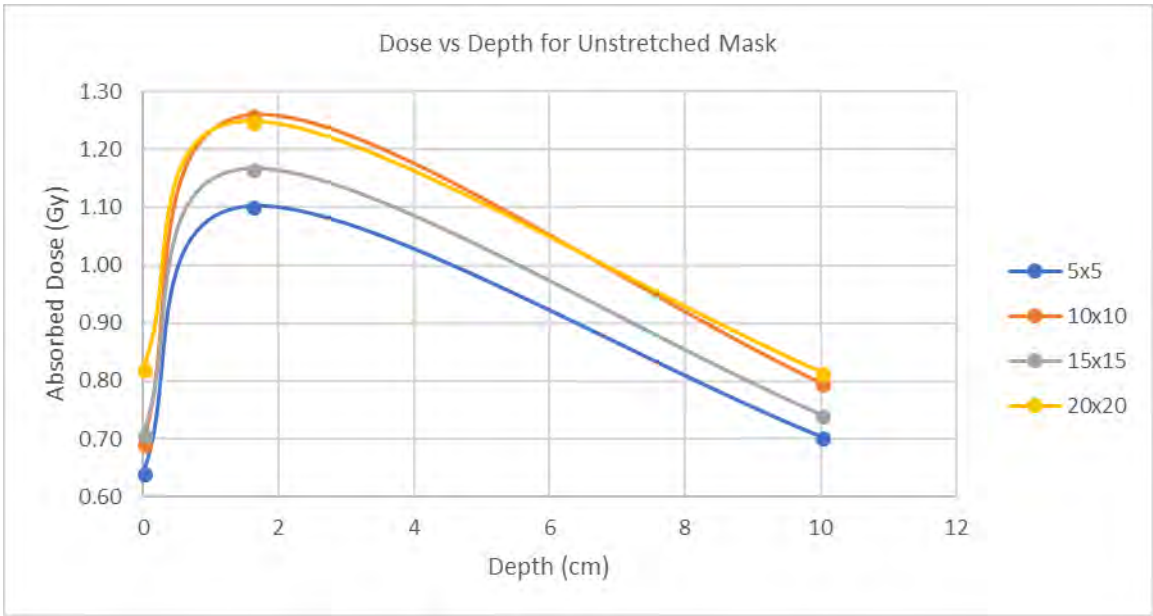

Figure 4. 17: A graph showing the variation of absorbed dose versus depth and field size for GafChromic measurements with the **unstretched mask**.

Figure 4. 18: A graph showing the variation of absorbed dose versus depth and field size for GafChromic measurements with the **5 cm stretched mask**.

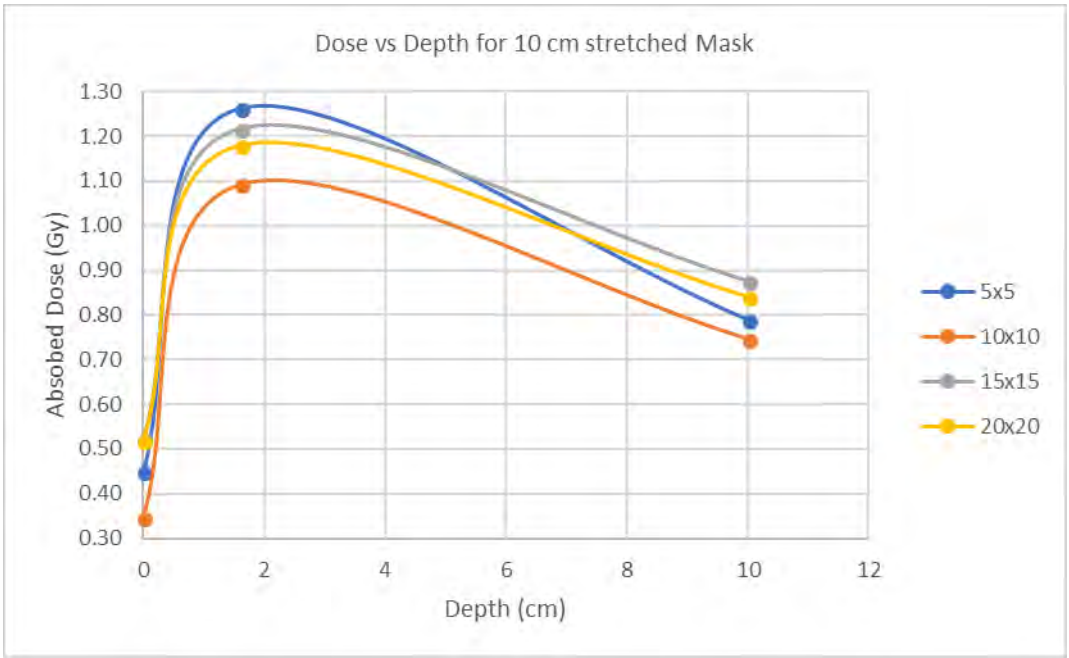

Figure 4. 19: A graph showing the variation of absorbed dose versus depth and field size for GafChromic measurements with the **10 cm stretched mask**.

CHAPTER FIVE

CONCLUSION AND RECOMMENDATIONS

5.1 Conclusions

The purpose of this research was to examine and analyze the effects of thermoplastic masks used as immobilization devices for cancer treatments in the head and neck region on the skin and the build-up region doses in terms of the thermoplastic percentage depth dose, thermoplastic factor and the changes in the skin dose and build-up region.

Taking into consideration measurements done with the ionization chamber, the surface dose, the dose at maximum depth (d_{max}) and the dose at a reference depth of 10 cm were found to increase with increasing mask thickness and increasing field size respectively. Due to the presence of the thermoplastic mask during measurements, the dose in the build-up region increased, subsequently shifting d_{max}, to increasingly lower depths to the skin surface. For a field size of 10 x 10 cm, an increase in skin dose of **0.21, 0.13 and 0.05 Gy** was estimated for the unstretched mask, the 5 cm stretched mask and the 10 cm stretched mask respectively, which was ascribed to the "bolus" effect of the thermoplastic masks. For the various field sizes, the skin dose increased by an average factor less than **1%** for the different mask stretches. However, a variation within 1% was recorded although the skin dose decreased as the mask was extended.

The thermoplastic factor at the skin surface was also found to increase with an increasing mask thickness and for a particular mask type (unstretched, 5 cm stretched, or 10 cm stretched) the thermoplastic factor decreased with increasing field size. With respect to the doses obtained using the GafChromic EBT3 films, there were lots of discrepancies in

the values which varied significantly with those obtained using the ionization chamber. The main cause behind the variation between the GafChromic EBT3 film and the ionization chamber dose values is the inhomogeneous composition of the GafChromic film emanating from the film's manufacturing process. Note that the film and the ion chamber measurements were yielding and comparing absolute dose values, that is, no normalization was applied.

It can generally be concluded that multiple factors contributed to the observed increase in skin dose during the measurements and these include, the bolus effect of the immobilization mask (the thickness of the mask use), the inadvertent inclusion of the skin as a part of the target volume and field size.

The results obtained from the dose verification using the anthropomorphic phantom and diodes clearly confirms the fact that the presence of the thermoplastic mask and increasing field size with or without the mask increases the skin dose. The percentage differences obtained were all less than 1% which falls within the tolerance limit of ±1%.

A vivid comparison of this work with that performed by (Adu-poku, 2017) a formal student of the Department of Medical Physics, on the "Dosimetric Effects of Thermoplastic Immobilizing Devices on Skin Dose" was done. It was found that the skin dose, the dose at maximum depth and at a reference depth of 10 cm, increased with increasing mask thickness and also increasing the field sizes respectively. With respect to the thermoplastic mask factor, both studies found that it increased at the skin surface as the mask thickness was increased and for a particular mask type (stretched or unstretched) the thermoplastic mask factor decreased with increasing field size. In both situations, the rise in dose was associated with the "bolus" effect caused by the presence

of the thermoplastic mask. Although, her work was performed on a Cobalt-60 (energy = 1.25 MeV) machine at Komfo Anokye Teaching Hospital, Kumasi, a variation within 1% was recorded although the skin dose decreased as the mask was extended for both studies.

5.2 Recommendations

At the Sweden Ghana Medical Center, when a thermoplastic mask is to be used at simulation, it should be stretched firmly toward the patient's skin surface to thin the polystyrene in the targeted area in order to minimize the bolus effect, the build-up effect and increase the skin sparing effect, bearing in mind not to compromise the rigidity of the mask as it will decrease the mask's capability to function properly as an immobilization device. Also, taking into account the skin as one of the sensitive structures will be possible to reduce the skin dose to a tolerable level without compromising the tumor target coverage during the treatment planning.

Since thermoplastic immobilization masks are said to increase the dose to the skin significantly, it is recommended that the thermoplastic mask factor should be incorporated into the treatment planning system, just as in tray factors, in order to account for the effect of the increase in skin dose.

5.3 Further Research

Additional work should be done using two different beam energies (example 6 MV and 15 MV) to study and compare the effect of the thermoplastic mask used as immobilizing device on skin dose.

REFERENCES

Adu-poku, O. (2017). *Dosimetric effects of thermoplastic immobilizing devices on skin dose.* University of Ghana, Legon. https://doi.org/10.1038/253004b0

Alnawaf, H., Butson, M., & Yu, P. K. N. (2012). Measurement and effects of MOSKIN detectors on skin dose during high energy radiotherapy treatment. *Australasian Physical & Engineering Sciences in Medicine*, *35*(3), 321–328. https://doi.org/10.1007/s13246-012-0153-1

Andreo, P., Almond, P. R., Mattsson, O., Nahum, A. E., & Roos, M. (1995). THE USE OF PLANE-PARALLEL IONIZATION CHAMBERS IN HIGH-ENERGY ELECTRON AND PHOTON BEAMS. AN INTERNATIONAL CODE OF PRACTICE FOR DOSIMETRY. *IAEA Technical Report Series*, *TRS-381*(December), 1–143.

Basics of Radiation Therapy | Clinical Gate. (2015). Retrieved February 8, 2018, from https://clinicalgate.com/basics-of-radiation-therapy-2/

Biggs, P. J., & Ling, C. C. (1979). Electrons as the cause of the observed dmax shift with field size in high energy photon beams. *Medical Physics*, *6*(4), 291–295. https://doi.org/10.1118/1.594580

Borca, V. C., Pasquino, M., Russo, G., Grosso, P., Cante, D., Sciacero, P., … Tofani, S. (2013a). Dosimetric characterization and use of GAFCHROMIC EBT3 film for IMRT dose verification. *Journal of Applied Clinical Medical Physics*, *14*(2), 158–171. https://doi.org/10.1120/jacmp.v14i2.4111

Borca, V. C., Pasquino, M., Russo, G., Grosso, P., Cante, D., Sciacero, P., … Tofani, S. (2013b). Dosimetric characterization and use of GAFCHROMIC EBT3 film for IMRT dose verification. *Journal of Applied Clinical Medical Physics*, *14*(2), 158–171. https://doi.org/10.1120/jacmp.v14i2.4111

Butson, M. J., Cheung, T., & Yu, P. K. N. (2007). Megavoltage x-ray skin dose variation with an angle using grid carbon fibre couch tops. *Physics in Medicine and Biology*, *52*(20), N485–N492. https://doi.org/10.1088/0031-9155/52/20/N03

Butson, M. J., Perez, M. D., Mathur, J. N., & Metcalfe, P. E. (1996). 6MV x-ray dose in the build up region: empirical model and the incident angle effect. *Australasian Physical & Engineering Sciences in Medicine*, *19*(2), 74–82. Retrieved from http://www.ncbi.nlm.nih.gov/pubmed/8826712

Butson, M. J., Yu, P. K. N., & Metcalfe, P. E. (1998). Measurement of off-axis and peripheral skin dose using radiochromic film. *Physics in Medicine and Biology*, *43*(9), 2647–2650. https://doi.org/10.1088/0031-9155/43/9/015

Butson, M. J., Yu, P. K. N., & Metcalfe, P. E. (1999). Extrapolated surface dose measurements with radiochromic film. *Medical Physics*, *26*(3), 485–488. https://doi.org/10.1118/1.598539

Butson, M., Mathur, J., & Metcalfe, P. (1997). Skin dose from radiotherapy X-ray beams: The influence of energy. *Australasian Radiology*, *41*(2), 148–150.

Chiu-Tsao, S. T., & Chan, M. F. (2009). Photon beam dosimetry in the superficial buildup region using radiochromic EBT film stack. *Medical Physics*, *36*(6), 2074–2083. https://doi.org/10.1118/1.3125134

Court, L. E., Tishler, R., Xiang, H., Allen, A. M., Makrigiorgos, M., & Chin, L. (2008). Experimental evaluation of the accuracy of skin dose calculation for a commercial treatment planning system. *Journal of Applied Clinical Medical Physics / American College of Medical Physics*, *9*(1), 2792.

De Ost, B., Vanregemorter, J., Schaeken, B., & Van Den Weyngaert, D. (1997). The effect of carbon fibre inserts on the build-up and attenuation of high energy photon beams. *Radiotherapy and Oncology*, *45*(3), 275–277. https://doi.org/10.1016/S0167-8140(97)00118-7

Dogan, N., & Glasgow, G. P. (2003). Surface and build-up region dosimetry for obliquely incident intensity modulated radiotherapy 6 MV x rays. *Medical Physics*, *30*(12), 3091–3096. https://doi.org/10.1118/1.1625116

Eliceiri, K. W., & Rueden, C. (2005). Tools for visualizing multidimensional images from living specimens. *Photochemistry and Photobiology*, *81*(5), 1116–1122. https://doi.org/10.1562/2004-11-22-IR-377

Fiorino, C., Cattaneo, G. M., del Vecchio, a, Longobardi, B., Signorotto, P., Calandrino, R., … Volterrani, F. (1992). Skin dose measurements for head and neck radiotherapy. *Medical Physics*, *19*(5), 1263–1266. https://doi.org/10.1118/1.596758

Gagnon, W. F., & Horton, J. L. (1979). Physical factors affecting absorbed dose to the skin from cobalt-60 gamma rays and 25-MV x rays. *Medical Physics*, *6*(4), 285–290. https://doi.org/10.1118/1.594583

Girish, V., Vijayalakshmi, a. (2004). Affordable Image Analysis using NIH Image / ImageJ. *Indian Journal of Cancer*, *41*(1), 47.

Hadley, S. W., Kelly, R., & Lam, K. (2004). Effects of immobilization mask material on surface dose. *Journal of Applied Clinical Medical Physics [Electronic Resource] / American College of Medical Physics.*, *6*(1), 1–7. https://doi.org/10.1120/jacmp.2023.25317

Hadley, S. W., Kelly, R., & Lam, K. (2005). Effects of immobilization mask material on surface dose. *Journal of Applied Clinical Medical Physics / American College of Medical Physics*, *6*(1), 1–7. https://doi.org/10.1120/jacmp.v6i1.1957

Higgins, D. M., Whitehurst, P., & Morgan, A. M. (2001). The effect of carbon fiber couch inserts on surface dose with beam size variation. *Medical Dosimetry*, *26*(3), 251–254. https://doi.org/10.1016/S0958-3947(01)00071-1

Hounsell, A. R., & Wilkinson, J. M. (1999). Electron contamination and build-up doses in conformal radiotherapy fields. *Physics in Medicine and Biology*, *44*(1), 43–55. https://doi.org/10.1088/0031-9155/44/1/005

Hsu, S.-H., Roberson, P. L., Chen, Y., Marsh, R. B., Pierce, L. J., & Moran, J. M. (2008). Assessment of skin dose for breast chest wall radiotherapy as a function of bolus material. *Physics in Medicine and Biology*, *53*(10), 2630. https://doi.org/10.1088/0031-9155/53/10/010

ICRP. (1977). Recommendations of the International Commission on Radiological Protection. ICRP Publication 26. *Annals of the ICRP*, *1*(3), 2–3. https://doi.org/10.1017/CBO9781107415324.004

ICRU. (1985). *ICRU Report 39: Determination of Dose Equivalents Resulting from External Radiation Sources*. Retrieved from papers3://publication/uuid/76C5448B-62FD-4031-A86D-AF520E686CD0

Jones, D. (1994). ICRU Report 50-Prescribing, Recording and Reporting Photon Beam Therapy. *Medical Physics*, *21*(6), 833–834. https://doi.org/10.1118/1.597396

Khan, F. M. (1971). Use of electron filter to reduce skin dose in cobalt teletherapy. *American Journal of Roentgenology*, *111*(1), 80–81.

Khan, F. M. (2014). *The Physics of Radiation Therapy* (5th Ed). Lippincott Williams & Wilkins.

Khan, F., Moore, V., & Levitt, S. (1973). Effect of various atomic number absorbers on skin dose for 10-MeV x-rays. *Radiol-ogy*, *109*, 209. https://doi.org/10.1148/109.1.209

Kim, S., Liu, C. R., Zhu, T. C., & Palta, J. R. (1998). Photon beam skin dose analyses for different clinical setups. *Medical Physics*, *25*(6), 860–866. https://doi.org/10.1118/1.598261

Klein, E. E., & Purdy, J. A. (1993). Entrance and exit dose regions for a clinac-2100c. *International Journal of Radiation Oncology, Biology, Physics*, *27*(2), 429–435. https://doi.org/10.1016/0360-3016(93)90256-U

Kron, T., & Ostwald, P. (1995). Skin exit dose in megavoltage x-ray beams determined by means of a plane parallel ionization chamber (Attix chamber). *Medical Physics*, *22*(5), 577–578. https://doi.org/10.1118/1.597544

Kry, S. F., Smith, S. A., Weathers, R., & Stovall, M. (2012). Skin dose during radiotherapy: A summary and general estimation technique. *Journal of Applied Clinical Medical Physics*, *13*(3), 20–34. https://doi.org/10.1118/1.3469011

Lamb, A., & Blake, S. (1998). Investigation and modelling of the surface dose from linear accelerator produced 6 and 10 MV photon beams. *Physics in Medicine and Biology*, *43*(5), 1133–1146. https://doi.org/10.1088/0031-9155/43/5/006

Lee, N., Chuang, C., Quivey, J. M., Phillips, T. L., Akazawa, P., Verhey, L. J., & Xia, P. (2002). Skin toxicity due to intensity-modulated radiotherapy for head-and-neck carcinoma. *International Journal of Radiation Oncology Biology Physics*, *53*(3), 630–637. https://doi.org/10.1016/S0360-3016(02)02756-6

Lewis, D. (2009). Gafchromic ® EBT2. *Isp*, 1–17.

Lewis, D., Micke, A., Yu, X., & Chan, M. F. (2012). An efficient protocol for radiochromic film dosimetry. *Medical Physics*, *39*(10), 6339. https://doi.org/10.1118/1.4754797

Lin, J.-P., Chu, T.-C., Lin, S.-Y., & Liu, M.-T. (2001). Skin dose measurement by using ultra-thin TLDs. *Applied Radiation and Isotopes*, *55*(3), 383–391. https://doi.org/10.1016/S0969-8043(01)00082-3

Marbach, J. R., & Almond, P. R. (1977). Scattered photons as the cause for the observed dmax shift with field size in high-energy photon beams. *Medical Physics*, *4*(4), 310–314. https://doi.org/10.1118/1.594319

Mellenberg, D. E. (1995). Dose behind various immobilization and beam-modifying devices. *International Journal of Radiation Oncology, Biology, Physics*, *32*(4), 1193–1197. https://doi.org/10.1016/0360-3016(94)00371-Q

Menegotti, L., Delana, A., & Martignano, A. (2008). Radiochromic film dosimetry with flatbed scanners: A fast and accurate method for dose calibration and uniformity correction with single film exposure. *Medical Physics*, *35*(7), 3078–3085. https://doi.org/10.1118/1.2936334

Meyer, L. (2014). What to Do When Radiation Causes Skin Damage. Retrieved February 18, 2018, from https://www.curetoday.com/publications/cure/2014/spring2014/what-to-do-when-radiation-causes-skin-damage

Musolino, S. V. (2000). *Absorbed Dose Determination in External Beam Radiotherapy: An International Code of Practice for Dosimetry Based on Standards of Absorbed Dose to Water; Technical Reports Series No. 398,. Health Physics* (Vol. 81). https://doi.org/10.1097/00004032-200111000-00017

Nichiporov, D., Kostjuchenko, V., Puhl, J. M., Bensen, D. L., Desrosiers, M. F., Dick, C. E., … Zink, S. (1995). Investigation of applicability of alanine and radiochromic detectors to dosimetry of proton clinical beams. *Applied Radiation and Isotopes*, *46*(12), 1355–1362. https://doi.org/10.1016/0969-8043(95)00213-W

Nilsson, B., & Brahme, A. (1986). Electron contamination from photon beam collimators. *Radiotherapy and Oncology : Journal of the European Society for Therapeutic Radiology and Oncology*, *5*(3), 235–244. https://doi.org/10.1016/S0167-8140(86)80053-6

Niroomand-Rad, A., Blackwell, C. R., Coursey, B. M., Gall, K. P., Galvin, J. M., Mclaughlin, W. L., … Soares, C. G. (1998). Radiochromic Film Dosimetry: Recommendation of AAPM Radiation Therapy Committe Task Group 55, *25*(11), 2093–2115.

Padikal, T. N., & Deye, J. A. (1978). Electron contamination of a high-energy x-ray beam. *Physics in Medicine and Biology*, *23*(6), 1086–1092. https://doi.org/10.1088/0031-9155/23/6/004

Panettieri, V., Barsoum, P., Westermark, M., Brualla, L., & Lax, I. (2009). AAA and

PBC calculation accuracy in the surface build-up region in tangential beam treatments. Phantom and breast case study with the Monte Carlo code penelope. *Radiotherapy and Oncology*, *93*(1), 94–101. https://doi.org/10.1016/j.radonc.2009.05.010

Pillai, K., Rao, P. S., & Gregg, E. C. (1973). Effect of shadow trays on surface dose and buildup for megavoltage radiation. *American Journal of Roentgenology*, *117*(1), 68–74.

Podgorsak, E. B., & Rosenberg, I. (2005). *Radiation Oncology Physics: A Handbook for Teachers and Students*. *International Atomic Energy Agency*. https://doi.org/10.1038/sj.bjc.6604224

Prabhu, L. (2012). Immobilization in radiotherapy. Retrieved from https://www.slideshare.net/prabhurt/immobilization-in-radiotherapy

Purdy, J. A. (1986). Buildup/surface dose and exit dose measurements for a 6-MV linear accelerator. *Medical Physics*, *13*(2), 259–262. https://doi.org/10.1118/1.595908

Rapley, P. (2006). Surface dose measurement using TLD powder extrapolation. *Medical Dosimetry*, *31*(3), 209–215. https://doi.org/10.1016/j.meddos.2006.02.003

Rawlinson, J. A., Arlen, D., & Newcombe, D. (1992). Design of parallel plate ion chambers for buildup measurements in megavoltage photon beams. *Medical Physics*, *19*(3), 641–648. https://doi.org/10.1118/1.596896

Sipilä, P., Ojala, J., Kaijaluoto, S., Jokelainen, I., & Kosunen, A. (2016). Gafchromic EBT3 film dosimetry in electron beams - energy dependence and improved film read-out. *Journal of Applied Clinical Medical Physics*, *17*(1), 360–373. https://doi.org/10.1120/jacmp.v17i1.5970

Stathakis, S., Li, J. S., Paskalev, K., Yang, J., Wang, L., & Ma, C. M. (2006). Ultra-thin TLDs for skin dose determination in high energy photon beams. *Physics in Medicine and Biology*, *51*(14), 3549–3567. https://doi.org/10.1088/0031-9155/51/14/018

Stevens, M. A., Turner, J. R., Hugtenburg, R. P., & Butler, P. H. (1996). High-resolution dosimetry using radiochromic film and a document scanner. *Physics in Medicine and Biology*, *41*(11), 2357–2365. https://doi.org/10.1088/0031-9155/41/11/008

Sweeney, R. (B. S., Bale, R. (M. D., Vogele, M., Nevinny-Stickel, M. (M. D., Bluhm, A. (R. T. T., Auer, T. (B. S., … Lukas, P. (M. D. (1998). Repositioning accuracy: Comparison of a noninvasive head holder with thermoplastic mask for fractionated radiotherapy and a case report. *International Journal of Radiation Oncology Biology Physics*, *41*(2), 475–483. https://doi.org/http://dx.doi.org/10.1016/S0360-3016(98)00064-9

Tabakov, S., Milano, F., Strand, S.-E., Lewis, C., & Sprawls, P. (2008). *Encyclopaedia of Medical Physics Volume I and II*.

Vatnitsky, S. M. (1997). Radiochromic film dosimetry for clinical proton beams. *Applied Radiation and Isotopes*, *48*(5), 643–651. https://doi.org/10.1016/S0969-8043(97)00342-4

Vatnitsky, S. M., Schulte, R. W. M., Galindo, R., Meinass, H. J., & Miller, D. W. (1997). Radiochromic film dosimetry for verification of dose distributions delivered with proton-beam radiosurgery, *1887*(42).

Velkley, D. E., Manson, D. J., Purdy, J. A., & Oliver, G. D. (1975). Build up region of megavoltage photon radiation sources. *Medical Physics*, *2*(1), 14–19. https://doi.org/10.1118/1.594158

Williams, J., & Thwaites, D. (2000). *Radiotherapy Physics: in Practice*. *Oxford University Press* (2nd Ed). Oxford University Press.

Yadav, G., Yadav, R. S., & Kumar, A. (2009). Skin dose estimation for various beam modifiers and source-to-surface distances for 6MV photons. *Journal of Medical Physics / Association of Medical Physicists of India*, *34*(2), 87–92. https://doi.org/10.4103/0971-6203.51935

Yu, P. K. N., Cheung, T., & Butson, M. J. (2003). Variations in skin dose using 6MV or 18MV x-ray beams. *Australasian Physical & Engineering Sciences in Medicine / Supported by the Australasian College of Physical Scientists in Medicine and the Australasian Association of Physical Sciences in Medicine*, *26*(2), 79–81. https://doi.org/10.1007/BF03178461

APPENDICES

APPENDIX 1

Data showing the physical thicknesses of the various thermoplastic masks with its corresponding hole dimensions.

APPENDIX 1A: Physical mask thicknesses with corresponding hole dimensions.

	Mask thickness (mm)	Hole diameter (mm)
Unstretched mask	2.30	-
5 cm stretched mask	1.20	2.30
10 cm stretched mask	0.86	5.25

APPENDIX 2

Raw data showing average electrometer readings (nC/min) with standard deviations on the solid water phantom measurements with and without the thermoplastic mask at various field sizes.

APPENDIX 2A: Electrometer readings without the mask.

Depth (cm)	Field Size (cm^2)			
	5x5	**10x10**	**15x15**	**20x20**
0	4.51 ± 0.00	5.25 ± 0.00	5.92 ± 0.00	6.62 ± 0.00
1.6	11.22 ± 0.01	11.81 ± 0.01	12.13 ± 0.01	12.39 ± 0.01
4	10.44 ± 0.01	11.17 ± 0.01	11.55 ± 0.01	11.83 ± 0.01
6	9.69 ± 0.00	10.51 ± 0.01	10.94 ± 0.01	11.26 ± 0.01
8	8.92 ± 0.00	9.83 ± 0.00	10.32 ± 0.01	10.68 ± 0.01
10	8.20 ± 0.00	9.15 ± 0.00	9.67 ± 0.00	10.05 ± 0.00

APPENDIX 2B: Electrometer readings with the unstretched mask.

Depth (cm)	Field Size (cm^2)			
	5x5	10x10	15x15	20x20
0	6.92 ± 0.01	7.68 ± 0.00	8.32 ± 0.00	8.95 ± 0.00
1.6	11.21 ± 0.01	11.82 ± 0.02	12.14 ± 0.01	12.42 ± 0.01
4	10.41 ± 0.01	11.13 ± 0.01	11.51 ± 0.01	11.78 ± 0.01
6	9.62 ± 0.00	10.45 ± 0.01	10.90 ± 0.01	11.23 ± 0.01
8	8.86 ± 0.00	9.74 ± 0.00	10.26 ± 0.01	10.62 ± 0.01
10	8.13 ± 0.00	9.08 ± 0.00	9.62 ± 0.00	10.01 ± 0.01

APPENDIX 2C: Electrometer readings with the 5 cm stretched mask.

Depth (cm)	Field Size (cm^2)			
	5x5	10x10	15x15	20x20
0	5.96 ± 0.00	6.72 ± 0.00	7.39 ± 0.00	8.05 ± 0.00
1.6	11.49 ± 0.00	12.09 ± 0.00	12.40 ± 0.01	12.66 ± 0.01
4	10.71 ± 0.01	11.43 ± 0.01	11.80 ± 0.01	12.09 ± 0.01
6	9.96 ± 0.00	10.77 ± 0.01	11.19 ± 0.01	11.50 ± 0.01
8	9.18 ± 0.00	10.09 ± 0.01	10.57 ± 0.01	10.91 ± 0.01
10	8.46 ± 0.00	9.40 ± 0.00	9.93 ± 0.00	10.29 ± 0.01

APPENDIX 2D: Electrometer readings with the 10 cm stretched mask.

Depth (cm)	Field Size (cm^2)			
	5x5	10x10	15x15	20x20
0	5.13 ± 0.00	5.89 ± 0.00	6.56 ± 0.00	7.25 ± 0.00
1.6	11.50 ± 0.01	12.11 ± 0.00	12.44 ± 0.01	12.70 ± 0.01
4	10.76 ± 0.01	11.47 ± 0.01	11.83 ± 0.00	12.11 ± 0.01
6	9.98 ± 0.00	10.81 ± 0.01	11.23 ± 0.01	11.55 ± 0.01
8	9.22 ± 0.00	10.11 ± 0.01	10.59 ± 0.01	10.93 ± 0.01
10	8.47 ± 0.00	9.41 ± 0.00	9.94 ± 0.00	10.31 ± 0.01

APPENDIX 3

Percentage Depth Dose (PDD) values for the ion chamber with and without the thermoplastic mask at various field sizes.

APPENDIX 3A: PDD values without the mask.

Depth (cm)	Field Size (cm^2)			
	5x5	10x10	15x15	20x20
0	40.19	44.42	48.82	53.47
1.6	100.00	100.00	100.00	100.00
4	93.05	94.53	95.22	95.53
6	86.42	89.00	90.19	90.88
8	79.54	83.18	85.08	86.19
10	73.13	77.41	79.71	81.14

APPENDIX 3B: PDD values with the unstretched mask.

Depth (cm)	Field Size (cm^2)			
	5x5	10x10	15x15	20x20
0	61.76	64.98	68.54	72.05
1.6	100.00	100.00	100.00	100.00
4	92.86	94.22	94.86	94.87
6	85.79	88.43	89.84	90.44
8	79.05	82.46	84.51	85.50
10	72.50	76.88	79.29	80.64

APPENDIX 3C: PDD values with the 5 cm stretched mask.

Depth (cm)	Field Size (cm^2)			
	5x5	10x10	15x15	20x20
0	51.89	55.61	59.56	63.63
1.6	100.00	100.00	100.00	100.00
4	93.24	94.57	95.16	95.50
6	86.64	89.11	90.24	90.89
8	79.88	83.43	85.19	86.23
10	73.61	77.78	80.02	81.27

APPENDIX 3D: PDD values with the 10 cm stretched mask.

Depth (cm)	Field Size (cm^2)			
	5x5	10x10	15x15	20x20
0	44.61	48.61	52.75	57.06
1.6	100.00	100.00	100.00	100.00
4	93.51	94.74	95.12	95.30
6	86.73	89.27	90.32	90.95
8	80.12	83.51	85.18	86.01
10	73.59	77.74	79.90	81.19

APPENDIX 4

Percentage Depth Dose (PDD) values at a depth of 0.0 cm for the various field sizes and mask stretches.

APPENDIX 4A: PDD values at the skin surface for the various field sizes and mask stretches.

Field sizes (cm^2)	Without Mask	Unstretched Mask	5 cm Stretched Mask	10 cm Stretched Mask
5X5	40.19	61.76	51.89	44.61
10X10	44.42	64.98	55.61	48.61
15X15	48.82	68.54	59.56	52.75
20X20	53.47	72.05	63.63	57.06

APPENDIX 5

Percentage Depth Dose (PDD) values against Depth for the various field sizes.

APPENDIX 5A: Field size of 5 x 5 cm^2

Depth (cm)	Without Mask	Unstretched Mask	5 cm Stretched Mask	10 cm Stretched Mask
0	40.19	61.76	51.89	44.61
1.6	100.00	100.00	100.00	100.00
4	93.05	92.86	93.24	93.51
6	86.42	85.79	86.64	86.73
8	79.54	79.05	79.88	80.12
10	73.13	72.50	73.61	73.59

APPENDIX 5B: Field size of 10 x 10 cm^2

Depth (cm)	Without Mask	Unstretched Mask	5 cm Stretched Mask	10 cm Stretched Mask
0	44.42	64.98	55.61	48.61
1.6	100.00	100.00	100.00	100.00
4	94.53	94.22	94.57	94.74
6	89.00	88.43	89.11	89.27
8	83.18	82.46	83.43	83.51
10	77.41	76.88	77.78	77.74

APPENDIX 5C: Field size of 15 x 15 cm^2

Depth (cm)	Without Mask	Unstretched Mask	5 cm Stretched Mask	10 cm Stretched Mask
0	48.82	68.54	59.56	52.75
1.6	100.00	100.00	100.00	100.00
4	95.22	94.86	95.16	95.12
6	90.19	89.84	90.24	90.32
8	85.08	84.51	85.19	85.18
10	79.71	79.29	80.02	79.90

APPENDIX 5D: Field size of 20 x 20 cm^2

Depth (cm)	Without Mask	Unstretched Mask	5 cm Stretched Mask	10 cm Stretched Mask
0	53.47	72.05	63.63	57.06
1.6	100.00	100.00	100.00	100.00
4	95.53	94.87	95.50	95.30
6	90.88	90.44	90.89	90.95
8	86.19	85.50	86.23	86.01
10	81.14	80.64	81.27	81.19

APPENDIX 6

Raw **RGB** data obtained after scanning and reading of the GafChromic EBT3 films for calibration.

APPENDIX 6A: Data from the red channel of the GafChromic EBT3 film

	Label	Area	Mean	StdDev	Min	Max
1	Cal001.tif (red):0086-0283	1600	94.611	0.826	93	98
2	Cal001.tif (red):0170-0281	1600	85.543	0.973	83	89
3	Cal001.tif (red):0252-0281	1600	78.973	0.831	75	81
4	Cal001.tif (red):0335-0281	1600	68.998	0.706	66	72
5	Cal001.tif (red):0414-0284	1600	56.981	0.76	55	62
6	Cal001.tif (red):0493-0282	1600	50.856	0.996	48	61
7	Cal001.tif (red):0577-0282	1600	47.254	0.938	45	64
8	Cal001.tif (red):0656-0282	1600	44.509	0.798	42	48
9	Cal001.tif (red):0742-0279	1600	42.047	0.958	38	46

APPENDIX 6B: Data from the green channel of the GafChromic EBT3 film

	Label	Area	Mean	StdDev	Min	Max
1	Cal001.tif (green):0086-0284	1600	128.862	0.907	126	133
2	Cal001.tif (green):0169-0282	1600	123.997	1.332	119	128
3	Cal001.tif (green):0250-0281	1600	119.659	1.021	115	123
4	Cal001.tif (green):0335-0279	1600	110.487	1.067	96	114
5	Cal001.tif (green):0413-0281	1600	96.182	0.92	94	99
6	Cal001.tif (green):0494-0282	1600	85.627	1.058	83	89
7	Cal001.tif (green):0574-0282	1600	77.557	0.882	74	84
8	Cal001.tif (green):0656-0281	1600	71.67	0.886	69	75
9	Cal001.tif (green):0742-0281	1600	64.387	0.758	62	67

APPENDIX 6C: Data from the blue channel of the GafChromic EBT3 film

	Label	Area	Mean	StdDev	Min	Max
1	Cal001.tif (blue):0086-0282	1600	71.726	0.803	69	76
2	Cal001.tif (blue):0170-0281	1600	71.556	0.906	69	75
3	Cal001.tif (blue):0249-0282	1600	70.962	0.836	68	75
4	Cal001.tif (blue):0334-0282	1600	69.189	0.813	62	72
5	Cal001.tif (blue):0413-0284	1600	66.206	0.798	64	70
6	Cal001.tif (blue):0493-0281	1600	63.684	1.152	60	74
7	Cal001.tif (blue):0575-0282	1600	61.845	0.881	60	66
8	Cal001.tif (blue):0654-0283	1600	59.981	0.839	58	64
9	Cal001.tif (blue):0740-0279	1600	57.641	0.785	55	60

APPENDIX 7

Raw data of the **red channel** obtained from the films irradiated with unknown doses for the various field sizes **without the thermoplastic mask**.

APPENDIX 7A: Field size of 5 x 5 cm^2

	Label	Area	Mean	StdDev	Min	Max
Unexposed	GWM 5x5001.tif (red):0155-0291	1600	93.039	0.987	90	97
A	GWM 5x5001.tif (red):0306-0275	1600	85.158	0.917	79	87
B	GWM 5x5001.tif (red):0457-0276	1600	62.183	2.063	30	73
C	GWM 5x5001.tif (red):0615-0276	1600	69.166	1.211	59	74

APPENDIX 7B: Field size of 10 x 10 cm^2

	Label	Area	Mean	StdDev	Min	Max
Unexposed	GWM 10x10002.tif (red):0128-0292	1600	92.453	0.79	90	96
A	GWM 10x10002.tif (red):0278-0286	1600	82.389	0.825	79	85
B	GWM 10x10002.tif (red):0423-0286	1600	60.093	0.975	58	79
C	GWM 10x10002.tif (red):0574-0282	1600	67.553	0.97	64	76

APPENDIX 7C: Field size of 15 x 15 cm^2

	Label	Area	Mean	StdDev	Min	Max
Unexposed	GWM 15x15003.tif (red):0136-0300	1600	93.982	0.971	91	97
A	GWM 15x15003.tif (red):0288-0281	1600	79.484	0.921	77	82
B	GWM 15x15003.tif (red):0457-0285	1600	61.156	0.845	59	68
C	GWM 15x15003.tif (red):0615-0283	1600	66.614	0.832	64	74

APPENDIX 7D: Field size of 20 x 20 cm^2

	Label	Area	Mean	StdDev	Min	Max
Unexposed	GWM 20x20004.tif (red):0136-0297	1600	91.922	0.818	90	95
A	GWM 20x20004.tif (red):0291-0285	1600	77.068	0.916	73	80
B	GWM 20x20004.tif (red):0449-0279	1600	60.008	1.61	34	78
C	GWM 20x20004.tif (red):0600-0288	1600	65.484	1.068	60	73

APPENDIX 8

Raw data of the **red channel** obtained from the films irradiated with unknown doses for the various field sizes with the **unstretched thermoplastic mask**.

APPENDIX 8A: Field size of 5 x 5 cm^2

	Label	Area	Mean	StdDev	Min	Max
Unexposed	GUM 5x5001.tif (red):0136-0301	1600	92.969	1.023	88	97
A	GUM 5x5001.tif (red):0282-0286	1600	70.627	2.48	62	76
B	GUM 5x5001.tif (red):0436-0288	1600	61.118	0.911	58	71
C	GUM 5x5001.tif (red):0578-0289	1600	68.869	1.734	62	73

APPENDIX 8B: Field size of 10 x 10 cm^2

	Label	Area	Mean	StdDev	Min	Max
Unexposed	GUM 10x10002.tif (red):0123-0288	1600	94.121	0.877	91	97
A	GUM 10x10002.tif (red):0266-0280	1600	70.021	1.701	66	75
B	GUM 10x10002.tif (red):0408-0285	1600	59.786	0.862	56	62
C	GUM 10x10002.tif (red):0552-0283	1600	67.452	0.928	64	71

APPENDIX 8C: Field size of 15 x 15 cm^2

	Label	Area	Mean	StdDev	Min	Max
Unexposed	GUM 15x15003.tif (red):0134-0299	1600	92.828	0.807	90	97
A	GUM 15x15003.tif (red):0279-0283	1600	68.656	1.17	65	73
B	GUM 15x15003.tif (red):0432-0289	1600	60.127	0.838	58	69
C	GUM 15x15003.tif (red):0578-0282	1600	67.821	0.927	65	75

APPENDIX 8D: Field size of 20 x 20 cm^2

	Label	Area	Mean	StdDev	Min	Max
Unexposed	GUM 20x20004.tif (red):0130-0295	1600	94.059	0.871	90	97
A	GUM 20x20004.tif (red):0279-0286	1600	66.856	1.043	63	70
B	GUM 20x20004.tif (red):0429-0284	1600	59.869	1.046	53	77
C	GUM 20x20004.tif (red):0572-0284	1600	66.994	0.915	64	70

APPENDIX 9

Raw data of the **red channel** obtained from the films irradiated with unknown doses for the various field sizes with the **5 cm stretched thermoplastic mask**.

APPENDIX 9A: Field size of 5 x 5 cm^2

	Label	Area	Mean	StdDev	Min	Max
Unexposed	GSS 5x5001.tif (red):0120-0293	1600	91.639	0.971	89	94
A	GSS 5x5001.tif (red):0253-0289	1600	75.046	2.152	71	82
B	GSS 5x5001.tif (red):0392-0286	1600	61.079	0.763	58	69
C	GSS 5x5001.tif (red):0527-0286	1600	68.109	0.779	66	71

APPENDIX 9B: Field size of 10 x 10 cm^2

	Label	Area	Mean	StdDev	Min	Max
Unexposed	GSS 10x10002.tif (red):0129-0290	1600	92.031	1.083	89	98
A	GSS 10x10002.tif (red):0265-0276	1600	72.863	1.498	69	78
B	GSS 10x10002.tif (red):0405-0284	1600	60.189	0.838	58	63
C	GSS 10x10002.tif (red):0544-0276	1600	67.268	0.981	58	71

APPENDIX 9C: Field size of 15 x 15 cm^2

	Label	Area	Mean	StdDev	Min	Max
Unexposed	GSS 15x15003.tif (red):0127-0298	1600	93.679	0.762	92	96
A	GSS 15x15003.tif (red):0268-0283	1600	72.993	1.416	69	78
B	GSS 15x15003.tif (red):0418-0285	1600	59.54	0.873	55	70
C	GSS 15x15003.tif (red):0564-0281	1600	66.114	0.95	62	69

APPENDIX 9D: Field size of 20 x 20 cm^2

	Label	Area	Mean	StdDev	Min	Max
Unexposed	GSS 20x20004.tif (red):0131-0295	1600	91.307	0.795	89	94
A	GSS 20x20004.tif (red):0281-0283	1600	71.17	1.668	66	76
B	GSS 20x20004.tif (red):0438-0284	1600	59.448	1.04	57	77
C	GSS 20x20004.tif (red):0589-0284	1600	66.555	0.966	60	73

APPENDIX 10

Raw data of the **red channel** obtained from the films irradiated with unknown doses for the various field sizes with the **10 cm stretched thermoplastic mask**.

APPENDIX 10A: Field size of 5 x 5 cm^2

	Label	Area	Mean	StdDev	Min	Max
Unexposed	GFS 5x5001.tif (red):0128-0289	1600	96.456	0.941	93	99
A	GFS 5x5001.tif (red):0252-0283	1600	79.873	2.585	75	86
B	GFS 5x5001.tif (red):0375-0280	1600	61.221	0.97	59	74
C	GFS 5x5001.tif (red):0495-0279	1600	69.296	0.895	67	73

APPENDIX 10B: Field size of 10 x 10 cm^2

	Label	Area	Mean	StdDev	Min	Max
Unexposed	GFS 10x10002.tif (red):0117-0281	1600	91.511	0.952	89	96
A	GFS 10x10002.tif (red):0245-0270	1600	79.478	2.357	73	84
B	GFS 10x10002.tif (red):0372-0270	1600	60.299	0.853	57	63
C	GFS 10x10002.tif (red):0500-0270	1600	66.765	0.936	64	70

APPENDIX 10C: Field size of 15 x 15 cm^2

	Label	Area	Mean	StdDev	Min	Max
Unexposed	GFS 15x15003.tif (red):0134-0276	1600	93.751	1.031	88	97
A	GFS 15x15003.tif (red):0261-0266	1600	75.044	2.125	70	80
B	GFS 15x15003.tif (red):0396-0271	1600	60.09	0.805	58	63
C	GFS 15x15003.tif (red):0532-0264	1600	65.53	1.079	60	75

APPENDIX 10D: Field size of 20 x 20 cm^2

	Label	Area	Mean	StdDev	Min	Max
Unexposed	GFS 20x20004.tif (red):0135-0293	1600	93.051	0.94	90	97
A	GFS 20x20004.tif (red):0262-0279	1600	74.578	1.836	63	79
B	GFS 20x20004.tif (red):0412-0283	1600	60.111	0.734	58	63
C	GFS 20x20004.tif (red):0540-0275	1600	65.756	0.912	61	71

APPENDIX 11

Data from dose verification in the head and neck region using the anthropomorphic phantom for a 6 MV photon energy.

APPENDIX 11A: Dose verification without the mask at the skin surface

Field size (cm^2)	Planned dose at d = 0.0 cm	Delivered dose at d = 0.0 cm	% Dev.	Tolerance
10 x 10	1.10	1.09	0.91	±1
20 x 20	1.12	1.11	0.89	±1

APPENDIX 11B: Dose verification with the mask at skin surface

Field size (cm^2)	Planned dose at d = 0.0 cm	Delivered dose at d = 0.0 cm	% Dev.	Tolerance
10 x 10	1.19	1.18	0.84	±1
20 x 20	1.23	1.22	0.81	±1

APPENDIX 11C: Dose verification without the mask at d_{max}

Field size (cm^2)	Planned dose at d = 1.6 cm	Delivered dose at d = 1.6 cm	% Dev.	Tolerance
10 x 10	1.38	1.37	0.72	±1
20 x 20	1.44	1.43	0.69	±1

APPENDIX 11D: Dose verification with the mask at d_{max}

Field size (cm^2)	Planned dose at d = 1.6 cm	Delivered dose at d = 1.6 cm	% Dev.	Tolerance
10 x 10	1.39	1.38	0.72	±1
20 x 20	1.45	1.45	0	±1